NASA MEMO 11-5-58L

NASA

MEMORANDUM

ANALYTICAL AND EXPERIMENTAL DETERMINATION OF THE COUPLED NATURAL FREQUENCIES AND MODE SHAPES OF A DYNAMIC MODEL OF A SINGLE-ROTOR HELICOPTER

By Milton A. Silveira and George W. Brooks

Langley Research Center
Langley Field, Va.

NATIONAL AERONAUTICS AND SPACE ADMINISTRATION
WASHINGTON
December 1958

F

NATIONAL AERONAUTICS AND SPACE ADMINISTRATION

MEMORANDUM 11-5-58L

ANALYTICAL AND EXPERIMENTAL DETERMINATION OF THE COUPLED NATURAL FREQUENCIES AND MODE SHAPES OF A DYNAMIC MODEL OF A SINGLE-ROTOR HELICOPTER

By Milton A. Silveira and George W. Brooks

SUMMARY

A combined analytical and experimental determination is made of the coupled natural frequencies and mode shapes in the longitudinal plane of symmetry for a dynamic model of a single-rotor helicopter. The analytical phase is worked out on the basis of a seven-degree-of-freedom system combining elastic deflections of the rotor blades, rotor shaft, pylon, and fuselage. The calculated coupled frequencies are first compared with calculated uncoupled frequencies to show the general effects of coupling and then with measured coupled frequencies to determine the extent to which the coupled frequencies can be calculated. The coupled mode shapes are also calculated and were observed visually with stroboscopic lights during the tests.

A comparison of the coupled and uncoupled natural frequencies shows that significant differences exist between these frequencies for some of the modes. Good agreement is obtained between the measured and calculated values for the coupled natural frequencies and mode shapes. The results show that the coupled natural frequencies and mode shapes can be determined by the analytical procedure presented herein with sufficient accuracy if the mass and stiffness distributions of the various components of the helicopter are known.

INTRODUCTION

It has become a well substantiated truth (for example, refs. 1 to 6) that helicopter rotors, when moving in forward flight, develop periodic aerodynamic loads which possess harmonic components having frequencies equal to all lower integral multiples of the rotational frequency of the rotor (the first 10 usually being of fundamental significance). It is also well known that the relative magnitudes of the harmonic components of the aerodynamic loading vary with rotor configuration and are strongly dependent on the helicopter flight velocity. These periodic aerodynamic forces produce undesirable vibrations in the helicopter which, in

conformity with the theory of vibrations, are dependent on the magnitude of the exciting force, the inherent or applied damping of the structure, and the nearness to resonance of the frequencies of the exciting forces with the natural frequencies.

The aerodynamic input forces and structural damping forces are controllable only to a limited extent and, thus, for practical purposes, the best way to avoid undesirable vibrations is to avoid conditions of resonance. In order to do this in a systematic and efficient manner, it is necessary to be able to predict the natural frequencies of the helicopter in flight. The frequencies referred to here are the coupled frequencies of the entire helicopter and not just the frequencies of the individual components.

A combined flight test and analytical investigation for a tandem helicopter is given in reference 7, wherein the natural frequencies, mode shapes, and vibration amplitudes in the longitudinal plane of symmetry are presented. The vibration amplitudes are presented for both in-flight aerodynamic forces and applied eccentric mass shaker forces. In the analytical investigation of the coupled natural frequencies therein, an attempt was made to select the more significant variables appropriate to that configuration in order to study the overall effects of coupling. Correlation between experimental and analytically predicted frequencies was good, but because the helicopter was not disassembled to obtain accurate evaluations of the mass and stiffness distributions of its components and inasmuch as the coupled mode shapes were not measured during flight tests, no precise evaluation of the adequacy of the assumptions in the theory could be made. Therefore, the decision was made to extend the investigation by means of dynamic-model studies wherein the structural properties of the components and the experimental coupled natural frequencies and mode shapes could be measured with sufficient accuracy to permit an evaluation of the theoretical approach.

This report presents the results of a combined experimental and analytical study of the coupled natural frequencies and mode shapes of a dynamic model. The specific purpose is to demonstrate that the general effects of coupling as outlined in reference 7 do exist, and that it is possible to predict, with reasonable accuracy, the coupled natural frequencies and mode shapes of the helicopter if the structural properties of the components are known. Although the experimental portion of the study was made under hovering conditions, the results are appropriate for any flight condition because the change in coupled frequencies and mode shapes with changes in flight conditions are believed to be negligible. In the analytical portion of this study, the theory of reference 7 is extended to include lateral-flexibility characteristics of the pylon and shaft.

In the organization of this report, the description of the model is first given in some detail. The reader who is interested primarily in the analysis may refer directly to the section entitled "Analytical Determination of Modes and Frequencies."

SYMBOLS

$A_1, A_2, \ldots$	coefficients of frequency determinant
a_1, a_2	coefficients of rotor-blade modal deflections
b_o	coefficient of rotor-shaft modal deflections
c_1	coefficient of pylon modal deflections
$d_o, \bar{d}_o, d_1$	coefficient of fuselage modal deflections
e	flapping hinge offset, in.
$(EI)_f$	structural stiffness of fuselage, lb-in.^{2}
$(EI)_p$	structural stiffness of pylon, lb-in.^{2}
$(EI)_r$	structural stiffness of rotor blades, lb-in.^{2}
F	length of fuselage, in.
f	longitudinal position of any fuselage element, in.
K_s	spring constant for shaft motions relative to the pylon, lb/in.
K_x	spring constant of mounts for vertical translation of fuselage, lb/in.
K_θ	spring constant of mounts for pitching motion of fuselage, lb-in./radian
K_1, K_2	Southwell coefficients for flapwise blade bending
M_F	mass of fuselage, lb-sec^2/in.

M_P mass of pylon, lb-sec^2/in.

M_Q mass of rotor shaft, lb-sec^2/in.

M_R mass of rotor blades, lb-sec^2/in.

M_d mass of dampers in upper pylon frame, lb-sec^2/in.

M_s mass of springs in upper pylon frame, lb-sec^2/in.

$M_{sd} = M_s + M_d$

$M_1, M_2, \ldots$ apparent mass terms in frequency determinant

m_f mass per unit length of fuselage, lb-sec^2/in.^{2}

m_p mass per unit length of pylon, lb-sec^2/in.^{2}

m_q mass per unit length of rotor shaft, lb-sec^2/in.^{2}

m_r mass per unit length of rotor blades, lb-sec^2/in.^{2}

$N_1, N_2, \ldots$ coefficients in frequency determinant

n number of blades

P vertical position of upper pylon frame, in.

p vertical position of any pylon element, in.

Q vertical position of rotor, in.

q vertical position of any rotor shaft element, in.

R rotor radius, in.

r radial position of any blade element, in.

T centrifugal force on the blade at any radial station, lb

$\overline{T}$ centrifugal force on the blade at any radial station divided by square of rotor speed, lb-sec^2

U	kinetic energy, lb-in.
u_1, u_2	uncoupled mode shapes for rotor blades
V	potential energy, lb-in.
v_o	uncoupled mode shape for a rotor shaft
w_1	uncoupled mode shape for pylon
$x_o, \bar{x}_o, x_1$	uncoupled mode shapes for fuselage
η	effective mass ratio
Ω	rotor speed, radians/sec
ω	natural frequency of coupled modes, radians/sec
$\omega_{(1)}, \omega_{(2)}, \ldots$	natural frequencies of first coupled mode, second coupled mode, . . .
ω_1	first natural uncoupled nonrotating flapwise bending frequency of rotor blades, radians/sec
ω_2	second natural uncoupled nonrotating flapwise bending frequency of rotor blades, radians/sec
ω_f	first natural uncoupled vertical bending frequency of fuselage, radians/sec
ω_p	first natural uncoupled bending frequency of pylon, radians/sec

Subscripts:

α	intersection of rotor shaft and rotor-disk plane
β	intersection of rotor shaft and upper pylon frame
γ	intersection of rotor shaft and horizontal plane of center of fuselage

Dots denote differentiation with respect to time, and primes denote differentiation with respect to length or space.

APPARATUS AND TESTS

General Description of Model

A general view of the model used in this investigation is shown in figure 1, details of the various components are shown in figures 2 to 6, and a sketch of the test configuration is shown in figure 7. The model was designed to possess the approximate dynamic properties of a 1/8-scale model of an existing helicopter. In this respect, the flapwise bending stiffness and mass distribution of the blades and the bending stiffness and mass distribution of the fuselage and pylon were scaled to yield a frequency spectrum representative of existing helicopters.

The model was designed for general dynamics studies, including the one discussed in the present report, and contains many provisions for variation of the significant parameters such as mass and stiffness distributions.

Description of Components

Rotor.- The rotor is a four-blade configuration with fully articulated blades. (See figs. 1, 2, and 4.) Motion of the blades about the drag hinges is damped by small viscous shear-type dampers (see figs. 3, 4, and 5) to avoid ground-resonance instabilities. Positive stops are also incorporated to limit blade motion in the plane of rotation to $\pm 12^{\circ}$. The collective pitch angles of the blades are adjusted individually by rotation of the blades in pitch at the blade root clamp. The pitch axis is located at 25 percent chord.

The rotor blades are of rectangular plan form and have a chord of 2.062 inches. The rotor has a diameter of 66 inches and a solidity of 0.08. The airfoil section is an NACA 0015 section. The blade spanwise weight distribution outboard of the root attachment is uniform with a chordwise center-of-gravity location at 32 percent chord. The blade structure consists of an aluminum leading-edge spar (see fig. 6) with balsa laminated to the spar to form the airfoil section. The flapwise bending stiffness of the rotor blades was scaled to be representative of existing helicopter rotor blades, whereas the torsional rigidity was maintained rather high to minimize the possibility of coupling between the flapwise bending and blade torsion. A trim tab attached to the trailing edge of the blade extending from station 30.5 to 31.5 and consisting of a small-gage wire frame covered with linen allows adjustment for blade tracking. Provisions for adjustment of the angular spacing between the blades and mass balance of the rotor system are obtained by the addition of weights to a balance rod shown in figure 4.

Pylon and rotor shaft.- The details of the pylon and rotor shaft are shown in figures 2 and 3. The pylon consists of a lower frame and upper frame which are connected by four vertical rods. The lower frame is rigidly attached to the fuselage. The upper pylon frame and the rotor shaft bearing housing are connected by four springs and dampers as shown in figures 2 and 3. The rotor shaft is connected at the top of the gear box (in the plane of the lower pylon frame) by means of a universal joint which permits the upper portion of the shaft to translate relative to the pylon. Thus, the flexibility of the shaft relative to the pylon is controlled by the four springs in the upper pylon frame. The flexibility of the entire pylon-shaft system relative to the fuselage is controlled by the stiffness of the four vertical pylon rods. This combination of springs and vertical rods provides a convenient method for variation of the natural frequencies of the pylon-shaft assembly.

The gear box at the lower end of the pylon is rigidly attached to the fuselage and transmits the torque from the horizontal shaft in the fuselage to the rotor shaft and, thence, to the rotor.

Fuselage and fuselage suspension.- The fuselage, shown in figure 1, was of box cross section and was constructed of two welded magnesium angles to provide the desired stiffness. The desired mass distribution is then obtained by the addition of mass as required. In simulating the fuselage, an attempt was made to obtain desired dynamic characteristics only, the geometry of the fuselage being secondary inasmuch as the rotor thrust was small and the aerodynamic effects on the natural frequencies and mode shapes negligible.

The fuselage was mounted on a very stiff cantilever beam, as shown in the sketch of figure 7, by means of two supports (front support and rear support) which permitted the model freedom of vertical translation and longitudinal pitching but provided a high relative restraint to other rigid-body motions. These supports were located at the approximate positions of the fuselage node points for fuselage first elastic free-free bending. The objective in using this type of support system was to duplicate as closely as possible the characteristics of a free-free system in the longitudinal plane of symmetry. During the model tests the configuration of the front support was found to be more desirable than the rear support (as shown in fig. 1), and subsequently the rear support was changed to be identical to the front support. The data presented in this paper were obtained with the latter support configuration (as shown in fig. 7).

Dampers.- The small dampers used to dampen motion of the blades about the drag hinge and the motion of the rotor shaft at the upper suspension plate of the pylon are of the shear type. The damper consists of a rod which slides through neoprene tubing. (See fig. 5.) A detailed description of the characteristics of this type of damper is given

in reference 8. Silicone oil is used as the damping fluid and the dampers provide a damping force which varies approximately as the square root of the velocity. The blade dampers also contain stops to limit rotor-blade-lag angles.

Model power supply.- The rotor system is driven by a compressed-air motor mounted in the center of the fuselage. A static pressure of 150 lb/sq in. is regulated by a gate control valve from which the air passes through a short flexible line to isolate vibration sources to the airline. The power output of the air motor is transmitted through a horizontal drive shaft to a commercial right-angle gear box which drives the rotor shaft.

Instrumentation.- Instrumentation of the model was accomplished by the use of accelerometers and electrical resistance-wire strain gages. The rotor-blade strains were indicated by flapwise bending and torsion strain gages located at $\frac{r}{R} = 0.38$. Strain gages mounted on small cantilever beams were used to measure pylon motions relative to the fuselage and rotor-shaft motions relative to the pylon. (See fig. 3.) Vertical translation and pitching motions of the fuselage were measured by accelerometers mounted on the fuselage and strain gages located at fuselage stations of $\frac{f}{F} = 0.33$ and 0.66 indicated fuselage vertical bending.

The strain-gage signals from the rotor are transmitted to the recording equipment through a slipring-brush assembly mounted on the rotor shaft as shown in figure 2.

An instantaneous value of the rotor speed was obtained by means of a commercial rotational-speed-indicating device which received signals from the small multipole generator operated from the gear box and shown just below the pylon in figure 1. A permanent record of the rotor speed was obtained from the signal of a one-per-revolution indicator mounted on the generator drive shaft.

Stroboscopic lighting was employed throughout the tests to obtain qualitative definition of the mode shapes associated with the various coupled natural frequencies.

All data were recorded on oscillograph records.

Evaluation of Component Structural Properties

Whenever possible in the method of analysis presented in this report, the equations are set up in a manner that permits the inclusion of the structural properties in terms of the spring constants, natural frequencies,

and mass distributions of the uncoupled components (blades, shaft, pylon, fuselage, and so forth). These component properties can, of course, be determined either experimentally or analytically, and in some instances, both procedures were used. However, greater emphasis was given to the experimental approach because it is felt that a similar procedure would lead to a more satisfactory evaluation of a full-scale helicopter. For example, the potential energy associated with the deflection of a rotor blade in a given mode shape is more readily determined by measuring the natural frequency and calculating the generalized mass for the particular mode than by integrating the product of the structural stiffness and the square of the blade curvature. In some instances, however, the experimental values were checked by the analytical methods presented in references 9, 10, and 11 to assure that these methods could be used to obtain sufficiently accurate results for preliminary calculations before components are available for testing or in the event that experimental test equipment is not available for component testing.

Prior to the assembly of the model, the natural frequencies of the individual components were determined experimentally. This was accomplished by mounting the component in such a manner as to simulate the assembled configuration (fixed-free condition for pylon, pin-end condition for blades, and so forth). The natural frequencies were then obtained by exciting the components with suitable shakers and noting the frequencies, as obtained from oscillograph records, where the deflection became a maximum.

Measurement of Coupled Natural Frequencies and Mode Shapes

After assembly of the model, the I-beam shown in figure 1 was mounted in a horizontal position on a rigid test bed in cantilever fashion as shown in figure 7. At a selected rotor speed, the frequency of the shaker output force was slowly varied from near zero up to the desired maximum value of approximately 300 radians per second. As the frequency was varied, the response of the various components was measured and recorded on oscillograph records. A simultaneous visual observation of the model was obtained by means of stroboscopic lights to obtain a qualitative value of the coupled natural frequencies as resonance conditions arose and to observe the corresponding coupled mode shapes. The rotor speed was then changed and the process repeated in order to obtain the variation of the coupled natural frequencies with rotor speed.

The coupled natural frequencies for each rotor speed were obtained from visual observations of the oscillograph records. A condition of

resonance was considered to exist at the frequencies where the response of the system became a maximum. These frequencies were then checked, wherever possible, against the values which produced maximum model deflections as determined by visual observations of the model under stroboscopic lighting. These visual observations were quite good for those modes involving large relative amplitudes of fuselage, pylon, and shaft motions but were of little use for modes involving large relative blade motions.

ANALYTICAL DETERMINATION OF MODES AND FREQUENCIES

General Considerations

The analysis of the coupled frequencies and mode shapes of the model employs the Lagrange energy-equation approach of reference 7. The analysis consists of writing the kinetic and potential energies of the structure in terms of the displacements of individual components. Although dampers were installed on the model to avoid ground-resonance instabilities, the effect of damping on the coupled frequencies is assumed to be of secondary importance. The calculation of the natural coupled frequencies is limited to the following degrees of freedom in the longitudinal plane of symmetry in order to reduce the complexity of the derivation: vertical translation, longitudinal pitching and structural bending of the fuselage, first and second flapwise bending of rotor blades, structural cantilever bending of the pylon, and rotation of the rotor shaft about the universal joint. In addition, an allowance is made for blade chordwise motions by assuming that the effective mass of the rotor blades in fore-and-aft translations of the rotor hub is ηM_R where η is generally less than unity. In the calculations of this paper, the effective mass ratio η is assumed to be 0.75.

Substitution of the energy equations into Lagrange's dynamic equations for free vibration yields the equations of motion from which the coupled frequencies and mode shapes are determined.

Energy Equations

The kinetic and potential energies are written in terms of the deflections of the components and their derivatives as follows:

Kinetic energy U

$$U = \frac{n}{2}\int_0^R m_r\left[\left(\dot{u} + \dot{x}_\gamma\right)^2 + \eta\left(\dot{v}_\alpha\right)^2\right]dr + \frac{1}{2}\int_0^Q m_q\left(\dot{v}^2 + \dot{x}_\gamma{}^2\right)dq +$$

$$\frac{1}{2}\int_0^P m_p\left(\dot{w}^2 + \dot{x}_\gamma{}^2\right)dp + \frac{1}{2}\int_0^F m_f\dot{x}^2df +$$

$$\frac{1}{2}\left(M_s + M_d\right)\left[\left(\frac{\dot{w}_\beta + \dot{v}_\beta}{2}\right)^2 + \dot{x}_\gamma{}^2\right] \tag{1}$$

Potential energy V

$$V = \frac{n}{2}\left[\int_0^R (EI)_r(u'')^2dr + \int_0^R T(u')^2dr\right] + \frac{1}{2}\int_0^P (EI)_p(w'')^2dp +$$

$$\frac{1}{2}\int_0^F (EI)_f(x'')^2df + Te\left(\frac{v_\alpha}{Q}\right)^2 + K_s\left(w_\beta - v_\beta\right)^2 +$$

$$\frac{1}{2}K_x d_o{}^2 + \frac{1}{2}K_\theta\left(\frac{2}{F}\bar{d}_o\right)^2 \tag{2}$$

where the dots denote derivatives with respect to time and the primes denote derivatives with respect to space or length. In equation (2), d_o represents rigid-body fuselage translation and $\frac{2}{F}\bar{d}_o$ represents rigid-body fuselage pitching.

The chosen deflections are shown in figure 7, along with α, β, and γ used as subscripts to designate the following positions on the model:

α intersection of rotor shaft and rotor-disk plane

β intersection of rotor shaft and upper pylon frame

γ intersection of rotor shaft and horizontal plane of center of fuselage

With the model mounted in its test configuration, there is a point between the front and rear fuselage supports at which a force applied vertically produces only fuselage vertical transformation and no fuselage longitudinal pitching. The spring constant K_x is the force per unit deflection for vertical forces applied at this point. The spring constant K_θ is the pitching moment per radian of fuselage rotation about this point for pitching moments applied in the longitudinal plane of symmetry. The front and rear fuselage supports were mounted so that this point coincides with the center of the fuselage (i.e., at $f/F = 0.5$). The helicopter in free flight would be represented by conditions of K_x and K_θ equal to zero.

Choice of Modes

The following equations express the deflections of the model in terms of the generalized coordinates and chosen mode shapes:

For blade first and second flapwise bending,

$$u = a_1 u_1 + a_2 u_2 \tag{3}$$

For rotor shaft translation and rotation about the universal joint,

$$v = b_o v_o - q x_\gamma' \tag{4}$$

For pylon bending and translation,

$$w = c_1 w_1 - p x_\gamma' \tag{5}$$

For fuselage translation, pitching, and bending,

$$x = d_o + \bar{d}_o \bar{x}_o + d_1 x_1 \tag{6}$$

where a_1, a_2, b_o, c_1, d_o, $\bar{d}_o$, and d_1 are unknown functions of time and u_1, u_2, v_o, w_1, x_o, and x_1 are the chosen mode shapes.

If the inclusion of additional modes in the analysis is desired, this is readily accomplished by the inclusion of the appropriate terms in equations (3) to (6) for the deflections of the various components. For example, third-mode bending of the blades could be included by the addition of the term a_3u_3 in equation (3).

Substitution of equations (3) to (6) into the energy equations (eqs. (1) and (2)) results in the following expressions for the kinetic and potential energies:

$$U = \frac{n}{2}\int_0^R m_r\left[\left(\dot{a}_1u_1 + \dot{a}_2u_2 + \dot{d}_o + \dot{\bar{d}}_o\bar{x}_{o,\gamma} + \dot{d}_1x_{1,\gamma}\right)^2 + \eta\left(\dot{b}_o + \dot{\bar{d}}_o\frac{2Q}{F} - Q\dot{d}_1x_{1,\gamma}'\right)^2\right]dr + \frac{1}{2}\int_0^Q mq\left[\left(\dot{b}_ov_o + \dot{\bar{d}}_o\frac{2q}{F} - \dot{d}_1qx_{1,\gamma}'\right)^2 + \left(\dot{d}_o + \dot{\bar{d}}_o\bar{x}_{o,\gamma} + \dot{d}_1x_{1,\gamma}\right)^2\right]dq + \frac{1}{2}\int_0^P m_p\left[\left(\dot{c}_1w_1 + \dot{\bar{d}}_o\frac{2p}{F} - \dot{d}_1px_{1,\gamma}'\right)^2 + \left(\dot{d}_o + \dot{\bar{d}}_o\bar{x}_{o,\gamma} + \dot{d}_1x_{1,\gamma}\right)^2\right]dp + \frac{1}{2}\int_0^F m_f\left(\dot{d}_o + \dot{\bar{d}}_o\bar{x}_o + \dot{d}_1x_1\right)^2df + \frac{1}{8}M_{sd}\left[\left(\dot{b}_ov_{o,\beta} + \dot{c}_1w_{1,\beta} + \dot{\bar{d}}_o\frac{4P}{F} - 2\dot{d}_1Px_{1,\gamma}'\right)^2 + 4\left(\dot{d}_o + \dot{\bar{d}}_o\bar{x}_{o,\gamma} + \dot{d}_1x_{1,\gamma}\right)^2\right] \tag{7}$$

$$V = \frac{n}{2}\left[\int_0^R (EI)_r\left(a_1u_1'' + a_2u_2''\right)^2dr + \int_0^R T\left(a_1u_1' + a_2u_2'\right)^2dr\right] + \frac{1}{2}\int_0^P (EI)_p\left(c_1w_1''\right)^2dp + \frac{1}{2}\int_0^F (EI)_f\left(d_1x_1''\right)^2df + T_e\left(\frac{b_o}{Q} + \frac{2}{F}\bar{d}_o - d_1x_{1,\gamma}'\right)^2 + K_s\left(c_1w_{1,\beta} - b_o\frac{P}{Q}\right)^2 + \frac{1}{2}K_xd_o^2 + \frac{2}{F^2}K_\theta\bar{d}_o^2 \tag{8}$$

The substitutions

$$\bar{x}_o = 1 - 2\frac{f}{F}$$

$$v_o = \frac{q}{Q}$$

$$v_\alpha = b_o + \bar{d}_o \frac{2Q}{F} - d_1 Q x'_{1,\gamma}$$

$$w_\beta - v_\beta = c_1 w_{1,\beta} - b_o \frac{P}{Q}$$

which consist of the fuselage pitching mode, the shaft horizontal deflections due to rotation about the universal joint, the total horizontal deflection of the center of the rotor hub, and the extension of the springs and dampers in the upper pylon frame, respectively, are used in the derivation of equation (8).

Derivation of Frequency Determinant

Some simplification is obtained by choosing natural modes for the uncoupled blade modes u_1 and u_2 and this choice is made in the analysis which follows. The differential equations of motion are determined by performing the operations indicated by Lagrange's equations for free vibrations on the energy equations as follows:

$$\left.\begin{aligned} \frac{d}{dt}\left(\frac{\partial U}{\partial \dot{a}_1}\right) - \left(\frac{\partial U}{\partial a_1}\right) + \frac{\partial V}{\partial a_1} = 0 \\ \frac{d}{dt}\left(\frac{\partial U}{\partial \dot{a}_2}\right) - \frac{\partial U}{\partial a_2} + \frac{\partial V}{\partial a_2} = 0 \\ \cdot \quad \cdot \quad \cdot \end{aligned}\right\} \tag{9}$$

where t denotes time.

The characteristic equations for free vibrations are found by considering harmonic motion, that is,

$$\left.\begin{aligned} a_1 &= \tilde{a}_1 \sin \omega t \\ a_2 &= \tilde{a}_2 \sin \omega t \\ &\cdot \quad \cdot \quad \cdot \quad \cdot \quad \cdot \end{aligned}\right\} \tag{10}$$

where the amplitudes of a_1, a_2, $\cdots$ are denoted by $\tilde{a}_o$, $\tilde{a}_1$, $\cdots$.

Substitution of equations (7) and (8) into equations (9) and making use of equations (10) leads to the characteristic equations which are given in matrix form as follows:

$$
\begin{bmatrix}
\left[1-\left(\frac{\omega_x}{\omega}\right)^2-K\left(\frac{\mu}{\omega_0}\right)^2\right]M_1 & 0 & 0 & 0 & A_1 & 0.6A_1 & 0.6A_1 \\
0 & \left[1-\left(\frac{\omega_y}{\omega}\right)^2-K_2\left(\frac{\mu}{\omega_0}\right)^2\right]M_2 & 0 & 0 & A_2 & 0.6A_2 & 0.6A_2 \\
0 & 0 & -\frac{\rho}{\omega^2}\left[\left(\frac{\mu}{\omega_0}\right)^2\overline{\tau}_0+\frac{K_{\theta\theta}}{\omega^2}\right]+N_1 & \frac{P}{\omega_0}\left[\frac{M_{\theta\theta}}{\omega}+\frac{K_{\theta\theta}}{\omega^2}\right] & 0 & 2\frac{P}{F}N_3-4\left(\frac{\mu}{\omega}\right)^2\frac{\overline{\tau}_e}{\omega_0 F} & 3.7\frac{P}{F}N_3-7.4\left(\frac{\mu}{\omega}\right)^2\frac{\overline{\tau}_e}{\omega_0 F} \\
0 & 0 & \frac{P}{\omega_0}\left[\frac{M_{\theta\theta}}{\omega}+\frac{K_{\theta\theta}}{\omega^2\overline{\tau}_0}\right] & \frac{M_{\theta\theta}}{\omega}-\frac{K_{\theta\theta}}{\omega^2}+\left[1-\left(\frac{\omega_y}{\omega}\right)^2\right]M_2 & 0 & 2\frac{P}{F}N_3 & 3.7\frac{P}{F}N_3 \\
A_1 & A_2 & 0 & 0 & N_1+M_F-\frac{K_x}{\omega^2} & 0.8N_4+A_4 & 0.6N_4+A_4 \\
0.8A_1 & 0.8A_2 & 2\frac{Q}{F}N_2-4\left(\frac{\mu}{\omega}\right)^2\frac{\overline{\tau}_e}{\omega_0 F} & 2\frac{P}{F}N_3 & 0.8N_4+A_4 & 0.74N_4+4.8\frac{Q^2}{F^2}N_4-\frac{1}{F^2}\left[\frac{K_\theta}{\omega^2}+2\left(\frac{\mu}{\omega}\right)^2\overline{\tau}_e\right]+M_3 & 0.48N_4+7.4\frac{Q^2}{F^2}N_4-\frac{7.4}{F^2}\left[2\left(\frac{\mu}{\omega}\right)^2\overline{\tau}_e\right]+A_4 \\
0.6A_1 & 0.6A_2 & 3.7\frac{Q}{F}N_2-7.4\left(\frac{\mu}{\omega}\right)^2\frac{\overline{\tau}_e}{\omega_0 F} & 3.7\frac{P}{F}N_3 & 0.6N_4+A_4 & 0.56N_4+7.4\frac{Q^2}{F^2}N_4-\frac{7.4}{F^2}\left[2\left(\frac{\mu}{\omega}\right)^2\overline{\tau}_e\right]+A_4 & 0.36N_4+14.8\frac{Q^2}{F^2}N_4-\frac{14.8}{F^2}\left[2\left(\frac{\mu}{\omega}\right)^2\overline{\tau}_e\right]+\left[1-\left(\frac{\omega_y}{\omega}\right)^2\right]M_4
\end{bmatrix}
\begin{Bmatrix}
\tilde{a}_1 \\ \tilde{a}_2 \\ \tilde{a}_3 \\ \tilde{a}_4 \\ \tilde{a}_5 \\ \tilde{a}_6 \\ \tilde{a}_7
\end{Bmatrix}
=
\begin{Bmatrix}
0 \\ 0 \\ 0 \\ 0 \\ 0 \\ 0 \\ 0
\end{Bmatrix}
\tag{11}
$$

where

$$A_1 = n \int_0^R m_r u_1 \, dr$$

$$A_2 = n \int_0^R m_r u_2 \, dr$$

$$A_3 = \frac{1}{P} \int_0^P m_p p w_1 \, dp$$

$$A_4 = \int_0^F m_f \bar{x}_o \, df$$

$$A_5 = \int_0^F m_f x_1 \, df$$

$$A_6 = \int_0^F m_f \bar{x}_o x_1 \, df$$

$$M_1 = n \int_0^R m_r u_1^2 dr$$

$$M_2 = n \int_0^R m_r u_2^2 dr$$

$$M_3 = \int_0^F m_f \bar{x}_o^2 df$$

$$M_4 = \int_0^F m_f x_1^2 df$$

$$M_5 = \frac{1}{P^2} \int_0^P m_p p^2 dp$$

$$M_6 = \int_0^P m_p w_1^2 dp$$

$$M_7 = \frac{1}{Q^2} \int_0^Q m_q q^2 dq$$

$$M_R = n \int_0^R m_r \, dr$$

$$M_P = \int_0^P m_p \, dp$$

$$M_Q = \int_0^Q m_q \, dq$$

$$M_F = \int_0^F m_f \, df$$

$$N_1 = \eta M_R + M_7 + \frac{M_{sd}}{4} \frac{P^2}{Q^2}$$

$$N_2 = \eta M_R + M_7 + \frac{M_{sd}}{2} \frac{P^2}{Q^2}$$

$$N_3 = A_3 + \frac{M_{sd}}{2}$$

$$N_4 = M_R + M_Q + M_P + M_{sd}$$

$$N_5 = \eta M_R + M_7 + \frac{P^2}{Q^2} M_5 + \frac{P^2}{Q^2} M_{sd}$$

The elements of the matrix (eq. (11)) contain all variables of the problem involving distributions of mass and stiffness. Substitution of the appropriate values for the model, derived from the model properties given in table I and figure 8, yields the following matrix, the elements of which contain the natural frequency ω, the rotor speed Ω, and the magnitudes of the generalized coordinates $\tilde{a}_1$, $\tilde{a}_2$, · · ·:

$$
\begin{bmatrix}
.00067845 - 1.71240\left(\frac{1}{\omega}\right)^2 - .0040706\left(\frac{\Omega}{\omega}\right)^2 & 0 & 0 & 0 & -.00065588 & -.00068470 & -.00051393 \\
0 & .0010626 - 22.98070\left(\frac{1}{\omega}\right)^2 + .015600\left(\frac{\Omega}{\omega}\right)^2 & 0 & 0 & .00097927 & .00078342 & .00058756 \\
0 & 0 & .0037685 - 103.33891\left(\frac{1}{\omega}\right)^2 - .00023494\left(\frac{\Omega}{\omega}\right)^2 & .000049126 + 131.99520\left(\frac{1}{\omega}\right)^2 & 0 & .00067442 - .000041620\left(\frac{\Omega}{\omega}\right)^2 & .0012645 - .000078037\left(\frac{\Omega}{\omega}\right)^2 \\
0 & 0 & .000049126 + 131.99520\left(\frac{1}{\omega}\right)^2 & .00187527 - 574.51224\left(\frac{1}{\omega}\right)^2 & 0 & .00018661 & .00034990 \\
-.00065588 & .00091327 & 0 & 0 & .044981 - 66.60000\left(\frac{1}{\omega}\right)^2 & .0028728 & .013483 \\
-.00068470 & .00078342 & .00067442 - .000041620\left(\frac{\Omega}{\omega}\right)^2 & .00018661 & .0028728 & .019379 - 14.39904\left(\frac{1}{\omega}\right)^2 - .000073734\left(\frac{\Omega}{\omega}\right)^2 & .0018097 - .000013824\left(\frac{\Omega}{\omega}\right)^2 \\
-.00051393 & .00058756 & .0012645 - .000078037\left(\frac{\Omega}{\omega}\right)^2 & .00034990 & .013483 & .0018097 - .000013824\left(\frac{\Omega}{\omega}\right)^2 & .012472 - 253.05620\left(\frac{1}{\omega}\right)^2 - .00002\times\times\left(\frac{\Omega}{\omega}\right)^2
\end{bmatrix}
\begin{Bmatrix}
\tilde{a}_1 \\ \tilde{a}_2 \\ \tilde{b}_0 \\ \tilde{b}_1 \\ \tilde{d}_2 \\ \tilde{d}_0 \\ \tilde{d}_1
\end{Bmatrix}
= 0 \qquad (12)
$$

Coupled Frequencies and Mode Shapes

The characteristic equation of the matrix, which yields the natural coupled frequencies, is obtained by setting the determinant of the matrix equal to zero. The assignment of unit value to one of the generalized coordinates then permits the evaluation of the other coordinates for each coupled frequency. The results presented in this report were obtained on automatic computing machines by the method of iteration which yields the coupled natural frequencies and generalized coordinates simultaneously. The mode shapes are then determined by the appropriate combinations of the generalized coordinates and the chosen modal functions as follows:

Fuselage vertical deflections:

$$x = \tilde{d}_o + \tilde{\bar{d}}_o\left(1 - 2\frac{f}{F}\right) + \tilde{d}_1 x_1 \tag{13}$$

Rotor-blade vertical deflections:

$$u = \tilde{d}_o + \tilde{\bar{d}}_o\left(1 - \frac{2f}{F}\gamma\right) + \tilde{d}_i x_{1,\gamma} + \tilde{a}_1 u_1 + \tilde{a}_2 u_2 \tag{14}$$

Rotor longitudinal deflections:

$$v_\alpha = \left(\tilde{\bar{d}}_o\frac{2}{F} - \tilde{d}_1 x_1'\right) Q + \tilde{b}_o \tag{15}$$

Pylon longitudinal deflections:

$$w = \left(\tilde{\bar{d}}_o\frac{2}{F} - \tilde{d}_1 x_{1,\gamma}'\right) p + \tilde{c}_1 w_1 \tag{16}$$

Shaft longitudinal deflections:

$$v = \left(\tilde{\bar{d}}_o\frac{2}{F} - \tilde{d}_1 x_{1,\gamma}'\right) q + \tilde{b}_o\frac{q}{Q} \tag{17}$$

The pylon and shaft vertical deflections are equal to the deflection of the fuselage at position γ, that is, x_γ.

For purposes of calculation, the mode shapes used for the components u_1, u_2, x_1, and w_1 were derived by fitting suitable approximate mathematical expressions to the normalized natural uncoupled mode shapes in order to obtain analytical expressions which are more readily integrable and differentiable. The resulting mode shapes are:

$$u_1 = \frac{r}{R} - 1.132 \sin \pi\frac{r}{R} + 0.026 \sin 2\pi\frac{r}{R} \tag{18}$$

$$u_2 = \frac{r}{R} - 0.647 \sin \pi\frac{r}{R} + 0.833 \sin 2\pi\frac{r}{R} + 0.1565 \sin 3\pi\frac{r}{R} \tag{19}$$

$$x_1 = -0.3 + 6.37\left(\frac{f}{F} - 0.5\right)^2 - 4.68\left(\frac{f}{F} - 0.5\right)^4 \tag{20}$$

$$w_1 = \left(\frac{p}{P}\right)^2 \tag{21}$$

The use of the approximate mode shapes for u_1 and u_2 do not admit exact conditions of orthogonality for these modes as implied in equations (11) and (12); however, the magnitudes of the cross-coupling terms which would exist are negligible and may be ignored. For example, the coefficient of $\left(\frac{\omega}{\Omega}\right)^2$ in the elements a_{12} and a_{21} of the matrix (eq. 12)), if included, would be less than 1 percent of the corresponding value for a_{11} and less than 0.2 percent of the corresponding value for a_{22}.

RESULTS AND DISCUSSION

The following section is divided into two parts. The first part presents the results of the calculated frequencies and mode shapes. The second part is devoted to a discussion of the comparison between calculated and measured results.

Calculated Results

Figure 9 shows the uncoupled natural frequencies of the model as a function of rotor speed. These frequencies were calculated by assuming all elements of the frequency determinant to be zero except those on the

principal diagonal and represent physically what would happen if elastic deformation occurred only in individual components of the structure. For example, the element a_{77} yields the fuselage uncoupled free-free elastic bending frequency under conditions wherein the blades, shaft, and pylon are rigid masses.

The curves of figure 9 show three points where the uncoupled natural frequencies coincide. Such a condition, of course, cannot exist for a physically coupled system. Figure 10 permits a comparison of the calculated uncoupled natural frequencies shown in figure 9 with the coupled natural frequencies derived from the complete frequency determinant. The modal coefficients which correspond to these coupled natural frequencies are presented in table II, and the mode shapes for a rotor speed of 23 radians per second are shown in the sketch of figure 11.

The rotor speed of 23 radians per second was chosen for plotting the mode shapes because of the substantial coupling indicated by figure 10 for rotor speeds in this region for the fifth and sixth coupled modes. The mode shapes for any other rotor speed are readily obtained by substitution of the coefficients from table II into equations (13) to (17).

The mode shapes shown in figure 11 are normalized by assigning a unit value to the point on the model having the maximum deflection for the respective mode and computing the relative deflections at other points. In plotting the mode shapes, the deflection of only one blade is shown since it is assumed in the analysis that all blades behave in a similar fashion. The scale for the deflections is substantially exaggerated relative to model lengths in order to point out the deflections associated with the various modes. The pylon deflections are shown as the dashed curves.

With reference to figures 10 and 11, the principal model deflections for the various coupled modes may be summarized as follows:

Mode 1 - fuselage pitching

Mode 2 - fuselage translation

Mode 3 - blade first elastic bending

Mode 4 - pylon bending and shaft translation

Mode 5 - blade second bending and fuselage bending

Mode 6 - blade second bending, shaft translation, pylon bending, and fuselage bending

Mode 7 - pylon bending

Although a seven-degree-of-freedom system was solved, attention is focused on the first six modes. The reason for this is as follows: In order to obtain a good representation of the lower coupled shaft-pylon mode (fourth coupled mode), the flexibility of the pylon was included in the analysis, along with the flexibility of the springs in the upper pylon frame. As a result, the higher mode, having a coupled frequency of approximately 688 radians per second and involving primarily pylon deflection, is obtained. This mode is included as a matter of information but the mode shape and frequency are only approximate because several uncoupled component modes (fuselage second elastic bending, blade third and fourth elastic bending, and so forth) having frequencies below the uncoupled frequency of the pylon have been neglected since the coupled frequencies which would result are above the region of primary concern (above the eighth harmonic of the rotor speed).

Comparison of Measured and Calculated Coupled Natural Frequencies

The main objective of this investigation was to derive the equations of motion for free vibrations by employing logical assumptions as to the primary degrees of freedom involved and to compare the calculated natural frequencies and mode shapes with those measured on the model to demonstrate that sufficient accuracy between calculated and measured results can be obtained.

Both the calculated and measured coupled natural frequencies are shown in figure 12. The calculated frequencies, repeated from figure 10, are shown as the dashed lines, and the measured values are given by the symbols. The results presented in figure 12 show good overall agreement between calculated and measured values for the coupled natural frequencies and indicate that the analytical procedure is adequate and that the modes chosen to represent the model structure are the important ones. Thus, it is concluded that the coupled natural frequencies and mode shapes can be determined by the analytical procedure presented herein with sufficient accuracy if the mass and stiffness distributions of the various helicopter components are known.

The analysis did not include damping of the components; however, dampers were installed on the model to avoid ground-resonance instabilities. The results show that substantial damping did exist as evidenced by the fact that, for values of the rotor speed where the coupled natural frequencies of two modes tended toward each other (e.g., modes 5 and 6 at $\approx$ 25 radians per second), it became increasingly difficult to locate the individual coupled frequencies on the oscillograph records. Instead, a large response of appropriate model components was noted over a rather

broad range of frequency of model excitation with but a single peak. Such situations are reminiscent of damped coupled systems (page 97 of ref. 9).

While the coupled natural frequencies were being measured, the coupled mode shapes were observed visually by means of stroboscopic lighting to ascertain that the relative motions of the components shown in figure 11 for the respective modes did exist. For the case of $\Omega = 0$, the vibrations of all model components could be readily observed; however, when the rotor was turning, rotor-blade motions could not be observed. Instead, the blade motions relative to fuselage motions were obtained from the oscillograph records of the rotor-blade and fuselage bending strains. In all cases, the agreement between the measured and calculated mode shapes was good but some differences were noted in the location of the node points.

CONCLUDING REMARKS

A dynamic model was constructed and tested, and an analytical procedure was devised to study the coupled natural frequencies and mode shapes of a single-rotor helicopter in the longitudinal plane of symmetry. The analytical study treats a seven-degree-of-freedom system involving elastic deformations of the rotor blades, rotor shaft, pylon, and fuselage and indicates a straightforward extension for the inclusion of additional degrees of freedom if desired. The elements of the frequency determinant are arranged to permit the uncoupled natural frequencies and mode shapes, which are often more conveniently determined experimentally, to be used to obtain the coupled values.

A comparison of the uncoupled and coupled natural frequencies for the model shows that significant differences exist between these frequencies for some of the modes, especially at rotor speeds where the natural frequencies for two uncoupled modes tend to coincide.

A comparison of the calculated coupled natural frequencies and mode shapes with those measured on the model shows good agreement and suggests that the significant variables are properly included in the analysis.

The coupled natural frequencies and mode shapes can be determined by the analytical procedure presented herein with sufficient accuracy if the mass and stiffness distributions of the various helicopter components are known.

Langley Research Center,
National Aeronautics and Space Administration,
Langley Field, Va., October 1, 1958.

REFERENCES

1. Mangler, K. W.: Calculation of the Induced Velocity Field of a Rotor. Rep. No. Aero. 2247, British R.A.E., Feb. 1948.

2. Mangler, K. W.: Fourier Coefficients for the Downwash at a Helicopter Rotor. Tech. Note Aero. 1958, British R.A.E., May 1948.

3. Hirsch, H., Kline, James, and Daughaday, Howard: An Experimental Investigation of the H-5 Variable Stiffness Blade Program. AF Tech. Rep. No. 6329, Pts. 1-6 (Contract W33-038 ac-14248 to Cornell Aero. Lab., Inc.), Wright Air Dev. Center, U. S. Air Force.
   Pt. 1 - Harmonic Reduction of Measured Blade Beam Bending Moment Data. Dec. 1951.
   Pt. 2 - Blade Beam Bending Moment Envelopes. Jan. 1952.
   Pt. 3 - Evaluation of Rotor Blade Resonant Bending Effects. Jan. 1952.
   Pt. 4 - Harmonic Reduction of Measured Blade-Motion and Control-Force Data. Apr. 1952.
   Pt. 5 - Evaluation of Blade Beam Bending Data Measured by Three Helicopter Manufacturers. June 1952.
   Pt. 6 - A Tentative Empirical Criterion for the Design of Rotor Blades for Higher Mode Resonances. Nov. 1952.

4. Daughaday, H., and Kline, J.: An Approach to the Determination of Higher Harmonic Rotor Blade Stresses. Proc. Ninth Annual Forum, Am. Helicopter Soc., Inc., May 14-17, 1953, pp. 90-126.

5. McCarty, John Locke, and Brooks, George W.: A Dynamic-Model Study of the Effect of Added Weights and Other Structural Variations on the Blade Bending Strains of an Experimental Two-Blade Jet-Driven Helicopter in Hovering and Forward Flight. NACA TN 3367, 1955.

6. Rabbott, John P., Jr., and Churchill, Gary B.: Experimental Investigation of the Aerodynamic Loading on a Helicopter Rotor Blade in Forward Flight. NACA RM L56I07, 1956.

7. Yeates, John E., Jr., Brooks, George W., and Houbolt, John C.: Flight and Analytical Methods for Determining the Coupled Vibration Response of a Tandem Helicopter. NACA Rep. 1326, 1957. (Supersedes NACA TN 3852 by Yeates and TN 3849 by Brooks and Houbolt.)

8. Silveira, Milton A., Maglieri, Domenic J., and Brooks, George W.: Results of an Experimental Investigation of Small Viscous Dampers. NACA TN 4257, 1958.

9. Den Hartog, J. P.: Mechanical Vibrations. Fourth ed., McGraw-Hill Book Co., Inc., 1956.

10. Houbolt, John C., and Anderson, Roger A.: Calculation of Uncoupled Modes and Frequencies in Bending or Torsion of Nonuniform Beams. NACA TN 1522, 1948.

11. Yntema, Robert T.: Simplified Procedures and Charts for the Rapid Estimation of Bending Frequencies of Rotating Beams. NACA TN 3459, 1955. (Supersedes NACA RM L54G02.)

TABLE I.- PARAMETERS OF BASIC CONFIGURATION

(a) Fuselage parameters

[K_x = 66.6 lb/in.; K_θ = 26,500 lb-in./radian; ω_f = 165.8 radians/sec; F = 85.8 in.]

Station	Fuselage location, f/F	Length of fuselage element, Δf, in.	Mass of fuselage element, $m_f \Delta f$, lb-sec^2/in.	First-bending-mode shape, x_1, in.
1	0.05	8.58	4.311×10^{-3}	0.798
2	.15	8.58	3.040	.410
3	.25	8.58	2.694	.080
4	.35	8.58	1.347	-.159
5	.45	8.58	5.301	-.284
6	.55	8.58	5.301	-.284
7	.65	8.58	1.305	-.159
8	.75	8.58	2.653	.080
9	.85	8.58	4.816	.410
10	.95	8.58	6.567	.798

(b) Blade parameters

[K_1 = 6.00; K_2 = 14.41; ω_1 = 50.24 radians/sec; ω_2 = 145.7 radians/sec; n = 4; R = 33 in.]

Station	Radial position, r/R	Length of blade element, Δr, in.	Mass of blade element, $m_r \Delta r$, lb-sec^2/in.	First-bending-mode shape, u_1, in.	Second-bending-mode shape, u_2, in.
1	0.05	3.24	0.255×10^{-3}	-0.119	0.292
2	.15	3.24	.218	-.343	.725
3	.25	3.24	.0614	-.524	.786
4	.35	3.24	.0614	-.638	.463
5	.45	3.24	.0614	-.660	-.056
6	.55	3.24	.0614	-.576	-.501
7	.65	3.24	.0614	-.379	-.665
8	.75	3.24	.0614	-.076	-.479
9	.85	3.24	.0614	.313	.004
10	.95	3.24	.0614	.764	.647

TABLE II.- MODAL COEFFICIENTS

	Modal coefficients for natural coupled frequencies -						
	$\omega(1)$	$\omega(2)$	$\omega(3)$	$\omega(4)$	$\omega(5)$	$\omega(6)$	$\omega(7)$
				$\Omega = 0$			
$\tilde{d}_1$	1.0000	1.0000	1.0000	1.0000	1.0000	1.0000	1.0000
$\tilde{a}_2$	3.1120	.5776	20.3270	.4114	20.6682	-.7166	-.4455
$\tilde{b}_o$	.8391	-.0482	2.9350	4.6829	-1.3659	-.7390	2.4971
$\tilde{c}_1$	.2188	-.0126	.7625	1.1364	-.3245	-.1626	-31.2945
$\tilde{d}_o$	8.0173	12.1254	77.3503	-.3172	-.7710	-.2889	-.2926
$\tilde{\tilde{d}}_o$	111.3020	-5.0030	90.5760	-.2424	-.8343	.0219	.2039
$\tilde{a}_1$	-49.3953	-14.8046	2226.7599	.1307	-1.1945	.4456	.5967
				$\Omega = 10$ radians/sec			
$\tilde{d}_1$	1.0000	1.0000	1.0000	1.0000	1.0000	1.0000	1.0000
$\tilde{a}_2$	2.9865	.5649	-14.9890	.3093	16.6571	-.8000	-.4471
$\tilde{b}_o$	.8502	-.0427	-2.4515	4.7001	-1.1523	-.7380	2.4969
$\tilde{c}_1$	.2230	-.0112	-.6353	1.1406	-.2718	-.1623	-31.2919
$\tilde{d}_o$	8.0264	12.1871	-46.8519	-.3147	-.6791	-.2869	-.2926
$\tilde{\tilde{d}}_o$	113.8169	-4.6444	-62.5789	-.2386	-.6766	.0255	.2039
$\tilde{a}_1$	-38.0329	-9.9922	-1595.6470	.1446	-.8984	.4601	.5976
				$\Omega = 20$ radians/sec			
$\tilde{d}_1$	1.0000	1.0000	1.0000	1.0000	1.0000	1.0000	1.0000
$\tilde{a}_2$	2.5907	.4923	-3.4053	.1786	8.8645	-1.1965	-.4517
$\tilde{b}_o$	.8603	-.0368	-.6998	4.7214	-.9006	-.7334	2.4962
$\tilde{c}_1$	.2264	-.00963	-.1799	1.1459	-.2080	-.1608	-31.2838
$\tilde{d}_o$	8.0482	12.2524	-7.7023	-.3113	-.5020	-.2777	-.2924
$\tilde{\tilde{d}}_o$	117.4951	-4.2756	-11.6857	-.2330	-.3640	.0424	.2041
$\tilde{a}_1$	-22.5308	-5.0411	-318.3830	.1789	-.2881	.5177	.6002
				$\Omega = 23$ radians/sec			
$\tilde{d}_1$	1.0000	1.0000	1.0000	1.0000	1.0000	1.0000	1.0000
$\tilde{a}_2$	2.4405	.4628	-2.6780	.1516	6.6173	-1.4822	-.4537
$\tilde{b}_o$	.8582	-.0356	-.5892	4.7258	-.8528	-.7301	2.4959
$\tilde{c}_1$	.2261	-.00933	-.1510	1.1469	-.1953	-.1597	-31.2802
$\tilde{d}_o$	8.0568	12.2643	-5.5902	-.3104	-.4512	-.2712	-.2924
$\tilde{\tilde{d}}_o$	118.3681	-4.2088	-8.6131	-.2315	-.2730	.05429	.2042
$\tilde{a}_1$	-19.1818	-4.1546	-238.4748	.1941	-.1010	.5529	.6014

TABLE II.- MODAL COEFFICIENTS - Continued

	Modal coefficients for natural coupled frequencies -						
	$\omega(1)$	$\omega(2)$	$\omega(3)$	$\omega(4)$	$\omega(5)$	$\omega(6)$	$\omega(7)$
				Ω = 26 radians/sec			
$\tilde{a}_1$	1.0000	1.0000	1.0000	1.0000	1.0000	1.0000	1.0000
$\tilde{a}_2$	2.2866	.4324	-2.1660	.1297	4.6415	-1.9499	-.4560
$\tilde{b}_o$	.8537	-.0346	-.5073	4.7295	-.8167	-.7248	2.4955
$\tilde{c}_1$	.2253	-.00908	-.1295	1.1479	-.1854	-.1579	-31.2762
$\tilde{d}_o$	8.0664	12.2737	-4.2260	-.3096	-.4068	-.2606	-.2923
$\tilde{d}_o$	119.1343	-4.1560	-6.5526	-.2300	-.1927	.0736	.2043
$\tilde{a}_1$	-16.4093	-3.4610	-183.8852	.2134	.0699	.6054	.6027
				Ω = 30 radians/sec			
$\tilde{d}_1$	1.0000	1.0000	1.0000	1.0000	1.0000	1.0000	1.0000
$\tilde{a}_2$	2.0838	.3924	-1.6694	.1069	2.6727	-3.0371	-.4596
$\tilde{b}_o$	.8442	-.0335	-.4162	4.7344	-.7853	-.7128	2.4950
$\tilde{c}_1$	.2234	-.00879	-.1056	1.1491	-.1765	-.1538	-31.2700
$\tilde{d}_o$	8.0807	12.2833	-3.0419	-.3084	-.3624	-.2364	-.2922
$\tilde{d}_o$	120.0194	-4.1020	-4.6971	-.2280	-.1124	-.1183	.2045
$\tilde{a}_1$	-13.4554	-2.7592	-133.6683	.2486	.2516	.7180	.6048
				Ω = 40 radians/sec			
$\tilde{d}_1$	1.0000	1.0000	1.0000	1.0000	1.0000	1.0000	1.0000
$\tilde{a}_2$	1.6281	.3031	-.8669	.0730	.8169	-7.5992	-.4711
$\tilde{b}_o$	.8054	-.0313	-.1157	4.7607	-.7590	-.6695	2.4933
$\tilde{c}_1$	.2149	-.00824	-.0288	1.1556	-.1687	-.1368	-31.2499
$\tilde{d}_o$	8.1250	12.2978	-1.5135	-.3034	-.3196	-.1356	-.2919
$\tilde{d}_o$	121.7831	-4.0179	-2.1783	-.2195	-.0343	.3047	.2050
$\tilde{a}_1$	-8.6354	-1.6892	-62.8946	.4766	.4943	1.1738	.6112
				Ω = 47 radians/sec			
$\tilde{d}_1$	1.0000	1.0000	1.0000	1.0000	1.0000	1.0000	1.0000
$\tilde{a}_2$	1.3679	.2526	-.4104	.0794	.4858	-10.7385	-.4816
$\tilde{b}_o$	.7668	-.0300	.9631	4.9620	-.7543	-.6449	2.4918
$\tilde{c}_1$	.2063	-.00792	.2353	1.2045	-.1672	-.1239	-31.2319
$\tilde{d}_o$	8.1633	12.3033	-.8732	-.2763	-.3102	-.0668	-.2916
$\tilde{d}_o$	122.8139	-3.9839	-1.0990	-.1779	-.0171	.4329	.2055
$\tilde{a}_1$	-6.6000	-1.2631	-30.1977	1.9250	.6356	1.4996	.6169

TABLE II.- MODAL COEFFICIENTS - Concluded

	Modal coefficients for natural coupled frequencies -						
	$\omega_{(1)}$	$\omega_{(2)}$	$\omega_{(3)}$	$\omega_{(4)}$	$\omega_{(5)}$	$\omega_{(6)}$	$\omega_{(7)}$
				Ω = 50 radians/sec			
$\tilde{d}_1$	1.0000	1.0000	------	--------	-------	1.0000	1.0000
$\tilde{a}_2$	1.2713	.2339	------	--------	-------	-11.9234	-.4868
$\tilde{b}_o$	.7476	-.02940	------	--------	-------	-.6366	2.4910
$\tilde{c}_1$	.2020	-.00779	------	--------	-------	-.1183	-31.2230
$\tilde{d}_o$	8.1816	12.3049	------	--------	-------	-.04094	-.2914
$\tilde{a}_o$	123.232	-3.9724	------	--------	-------	.4812	.2057
$\tilde{a}_1$	-5.9361	-1.1273	------	--------	-------	1.6266	.6197
				Ω = 55 radians/sec			
$\tilde{d}_1$	1.0000	1.0000	1.0000	1.0000	1.0000	1.0000	1.0000
$\tilde{a}_2$	1.1281	.2064	.0285	-.3565	.3220	-13.6803	-.4964
$\tilde{b}_o$	.7122	-.0285	4.5773	-1.5437	-.7507	-.6251	2.4896
$\tilde{c}_1$	.1940	-.00757	1.1116	-.3680	-.1660	-.1090	-31.2065
$\tilde{d}_o$	8.2147	12.3070	-.3235	-.8128	-.3021	-.00268	-.2911
$\tilde{a}_o$	123.9158	-3.9573	-.2478	-.9036	-.00236	.5530	.2061
$\tilde{a}_1$	-5.0292	-.9441	-.6437	-27.4793	.8960	1.8193	.6248
				Ω = 60 radians/sec			
$\tilde{d}_1$	1.0000	1.0000	1.0000	1.0000	1.0000	1.0000	1.0000
$\tilde{a}_2$	1.0030	.1827	.0277	-.1650	.2689	-15.1884	-.5074
$\tilde{b}_o$	.6726	-.0275	4.6118	-1.0479	-.7476	.6160	2.4880
$\tilde{c}_1$	.1891	-.00734	1.1200	-.2456	-.1650	-.0993	-31.1879
$\tilde{d}_o$	8.2510	12.3084	-.3177	-.6043	-.2955	.0301	-.2908
$\tilde{a}_o$	124.5971	-3.9459	-.2384	-.5450	.00983	.6147	.2066
$\tilde{a}_1$	-4.3139	-.8014	-.3372	-16.1398	1.2047	1.9894	.6305
				Ω = 70 radians/sec			
$\tilde{d}_1$	1.0000	1.0000	1.0000	1.0000	1.0000	1.0000	1.0000
$\tilde{a}_2$	.8082	.1451	.0226	.0460	.2457	-17.5897	-.5342
$\tilde{b}_o$	.5812	-.0256	4.6141	-.8164	-.7293	-.6034	2.4841
$\tilde{c}_1$	.1644	-.00688	1.1209	-.1850	-.1590	-.0779	-31.1431
$\tilde{d}_o$	8.3336	12.3097	-.3144	-.3935	-.2600	.0821	-.2900
$\tilde{a}_o$	129.9960	-3.9287	-.2316	-.1685	.0748	.7129	.2078
$\tilde{a}_1$	-3.2747	-.5973	-.1648	-4.4599	3.1509	2.2698	.6439

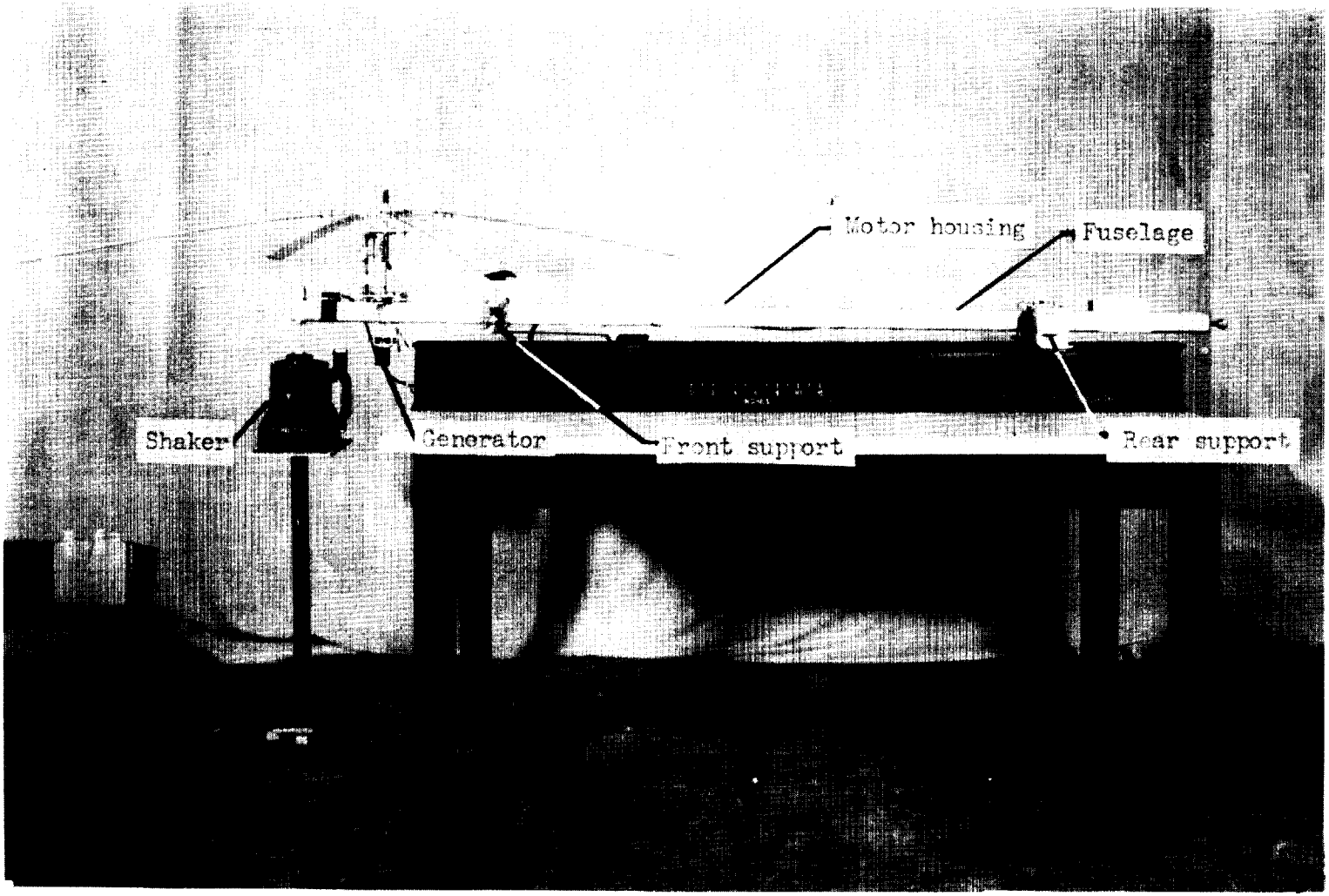

Figure 1.- Side view of model showing general methods of shaker installation and fuselage mounting. L-95196.1

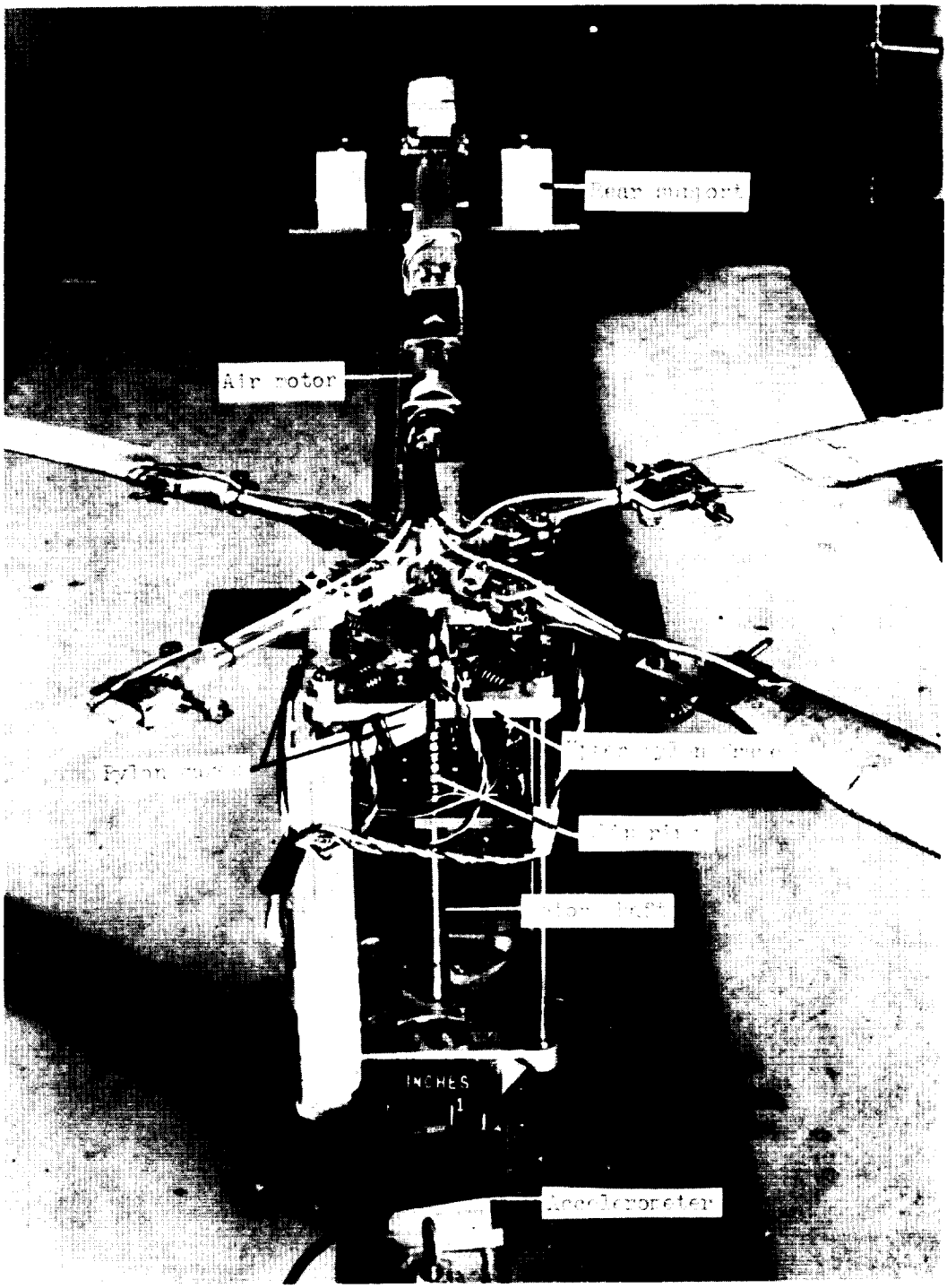

Figure 2.- Front view of the model. L-95197.1

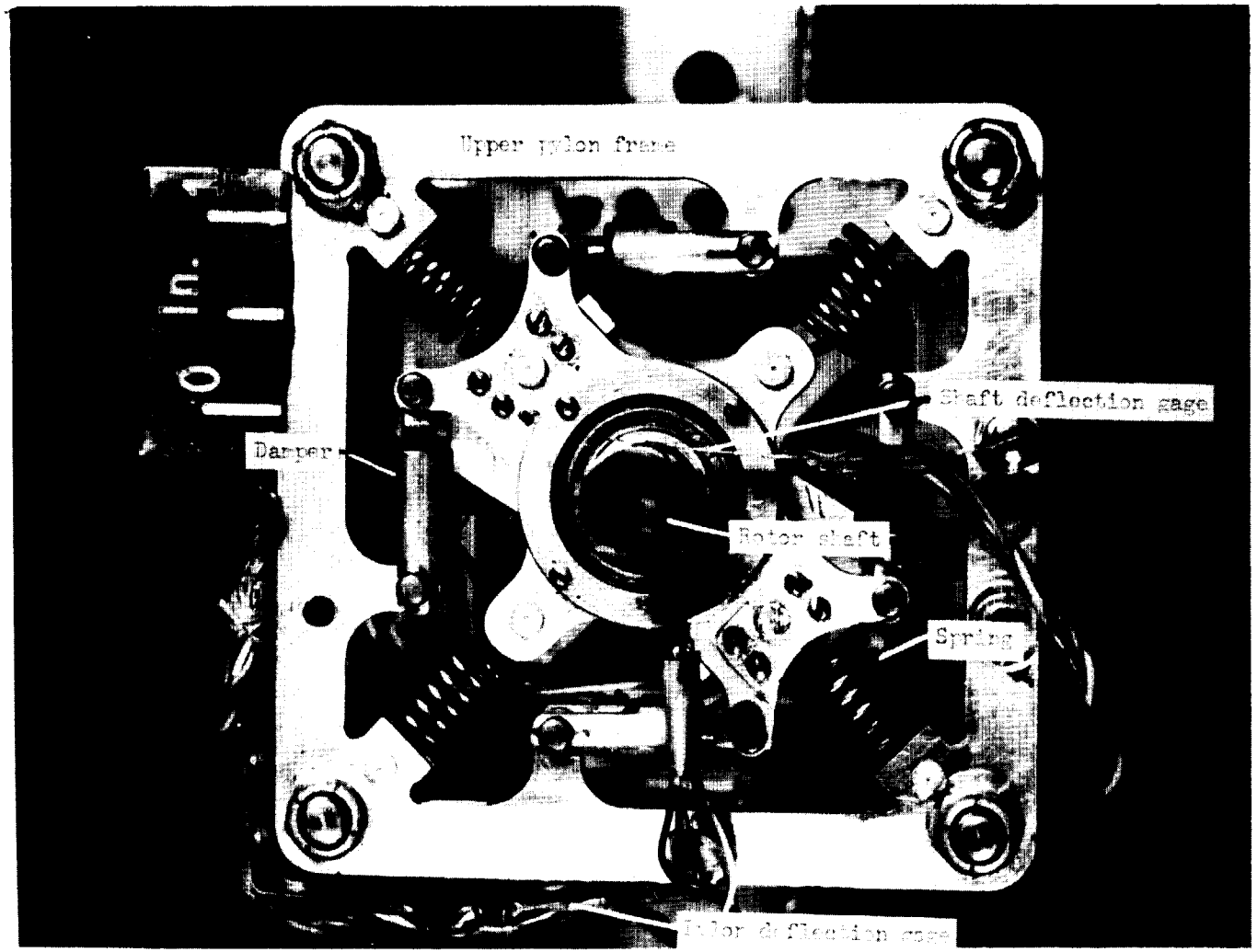

Figure 3.- Top view of pylon and shaft showing details of spring and damper installations in upper pylon frame. L-95198.1

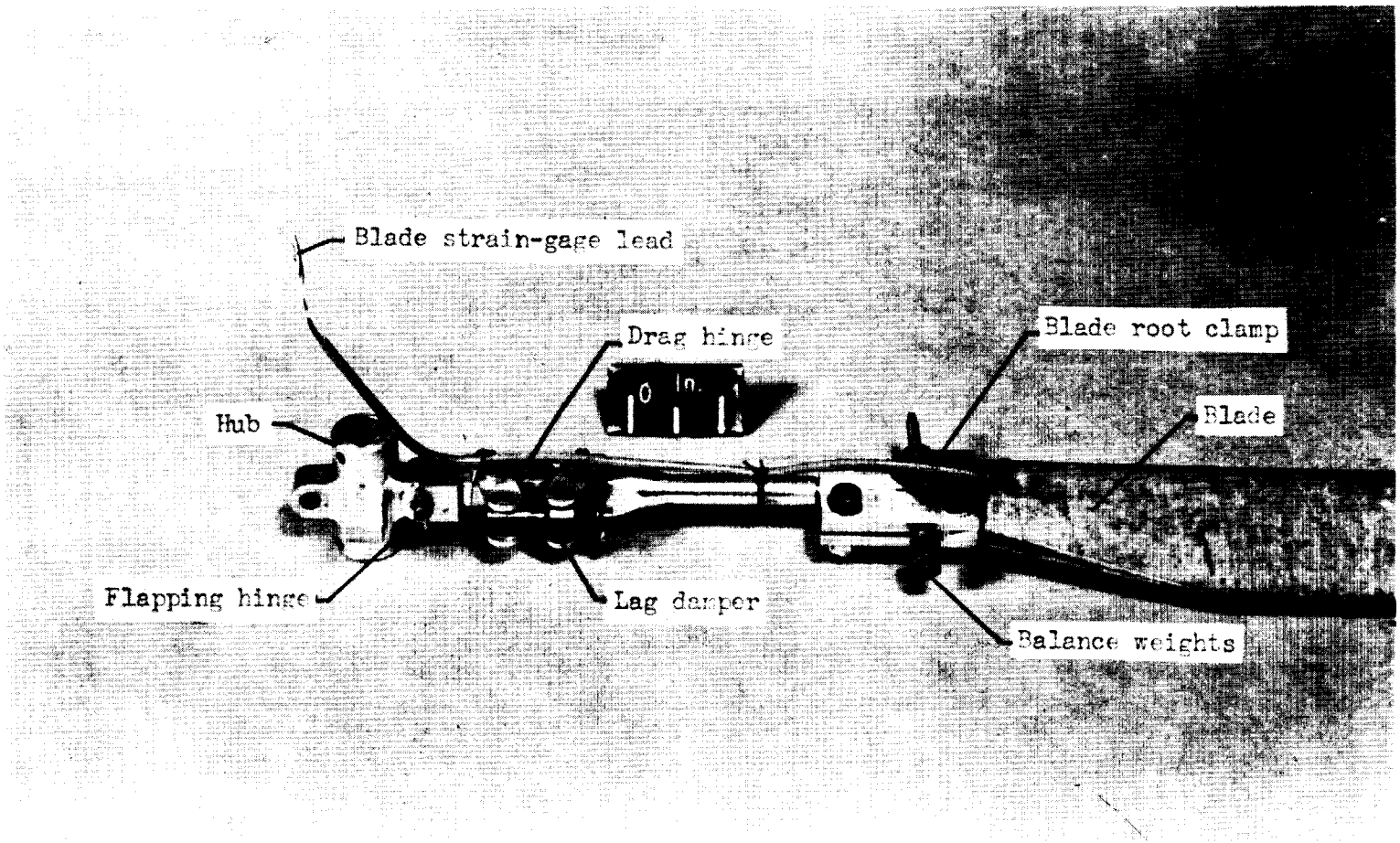

Figure 4.- Hub and inboard section of rotor blade. L-95200.1

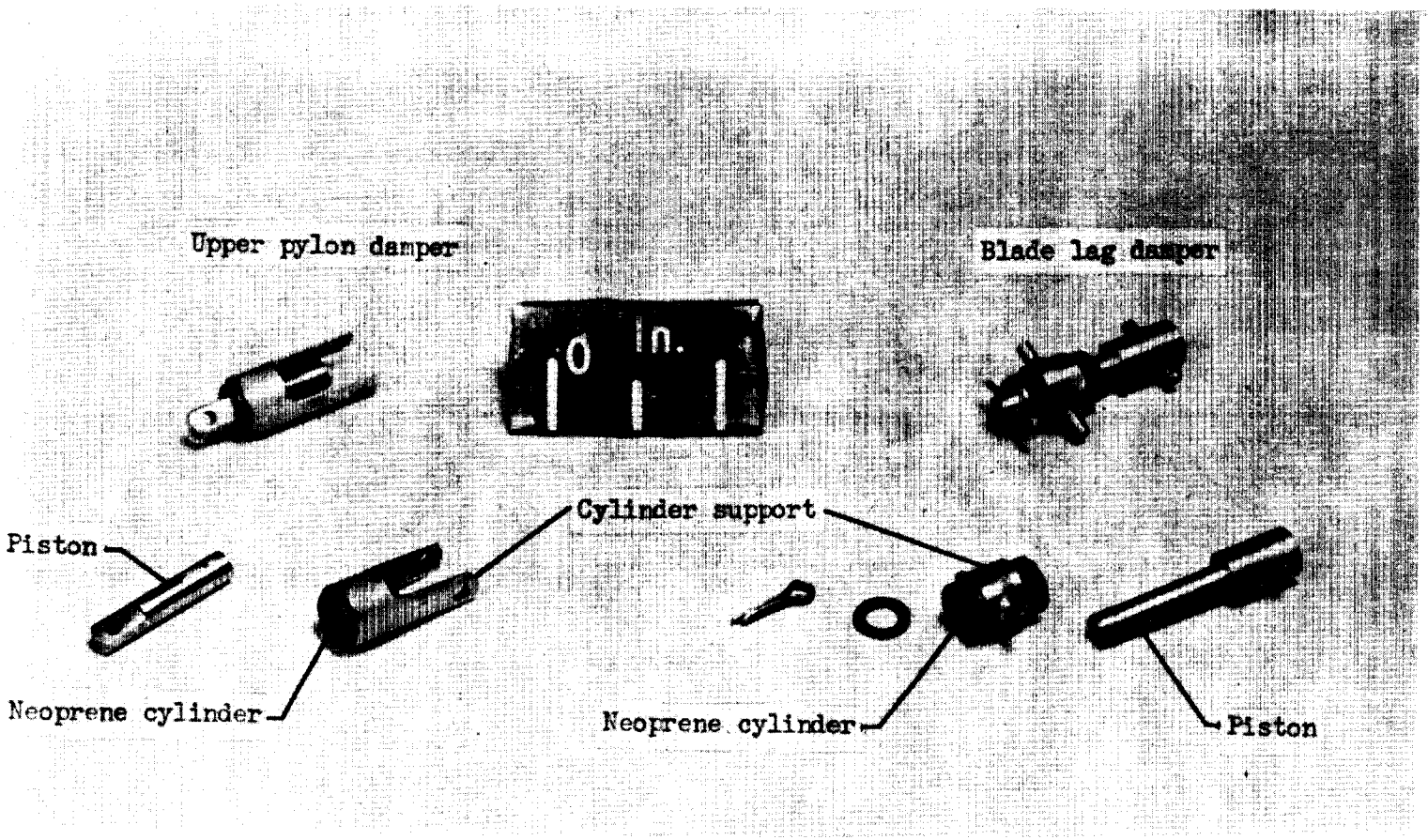

Figure 5.- Details of upper pylon and blade lag dampers (assembled and disassembled). L-95202.1

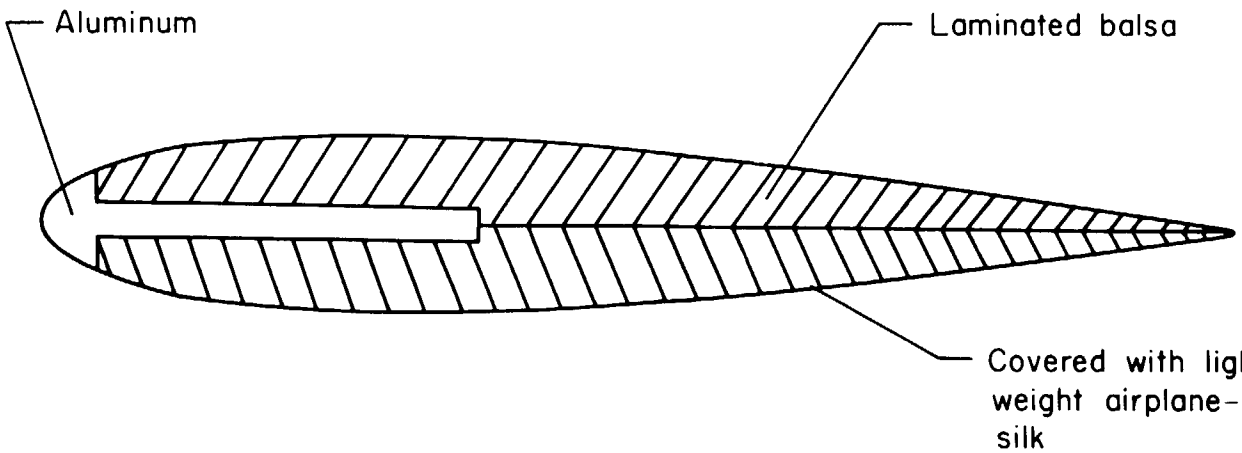

Airfoil section	NACA 0015
Chord	2.062 in.
Chordwise center of gravity	32 % chord

Figure 6.- Airfoil section.

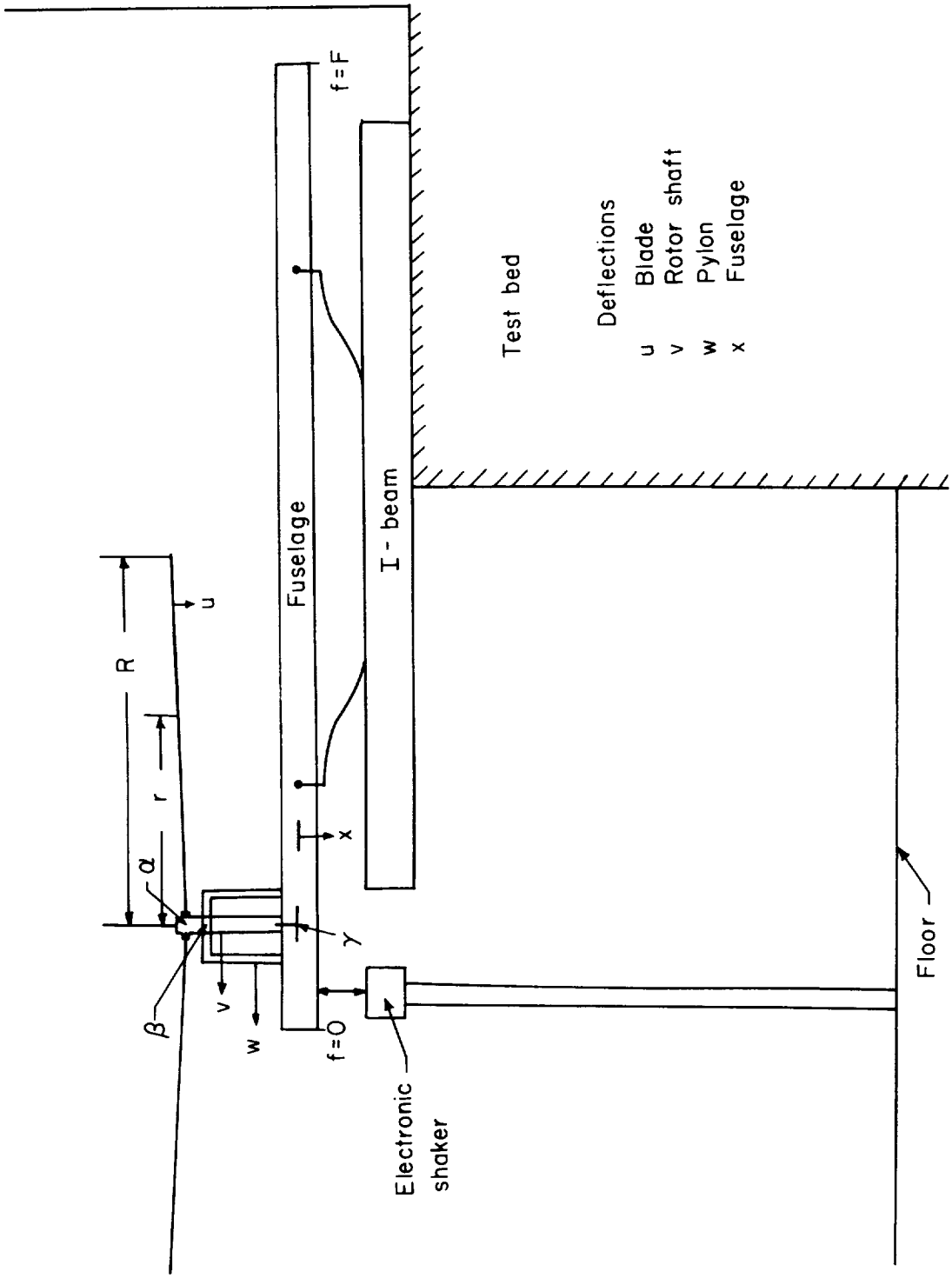

Figure 7.- Sketch showing direction of positive deflections of model test configuration.

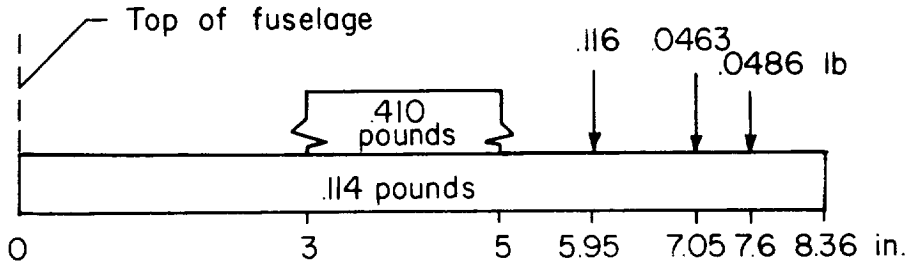

(a) Mass distribution of rotor shaft.

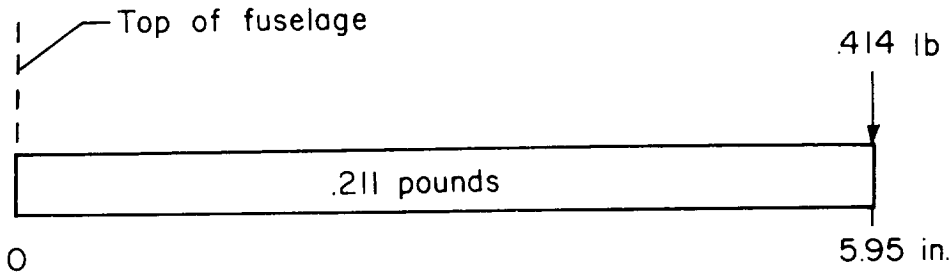

(b) Mass distribution of pylon. K_s = 84.3 pounds per inch; w_p = 584.04 radians per second.

Figure 8.- Mass distributions of rotor shaft and pylon.

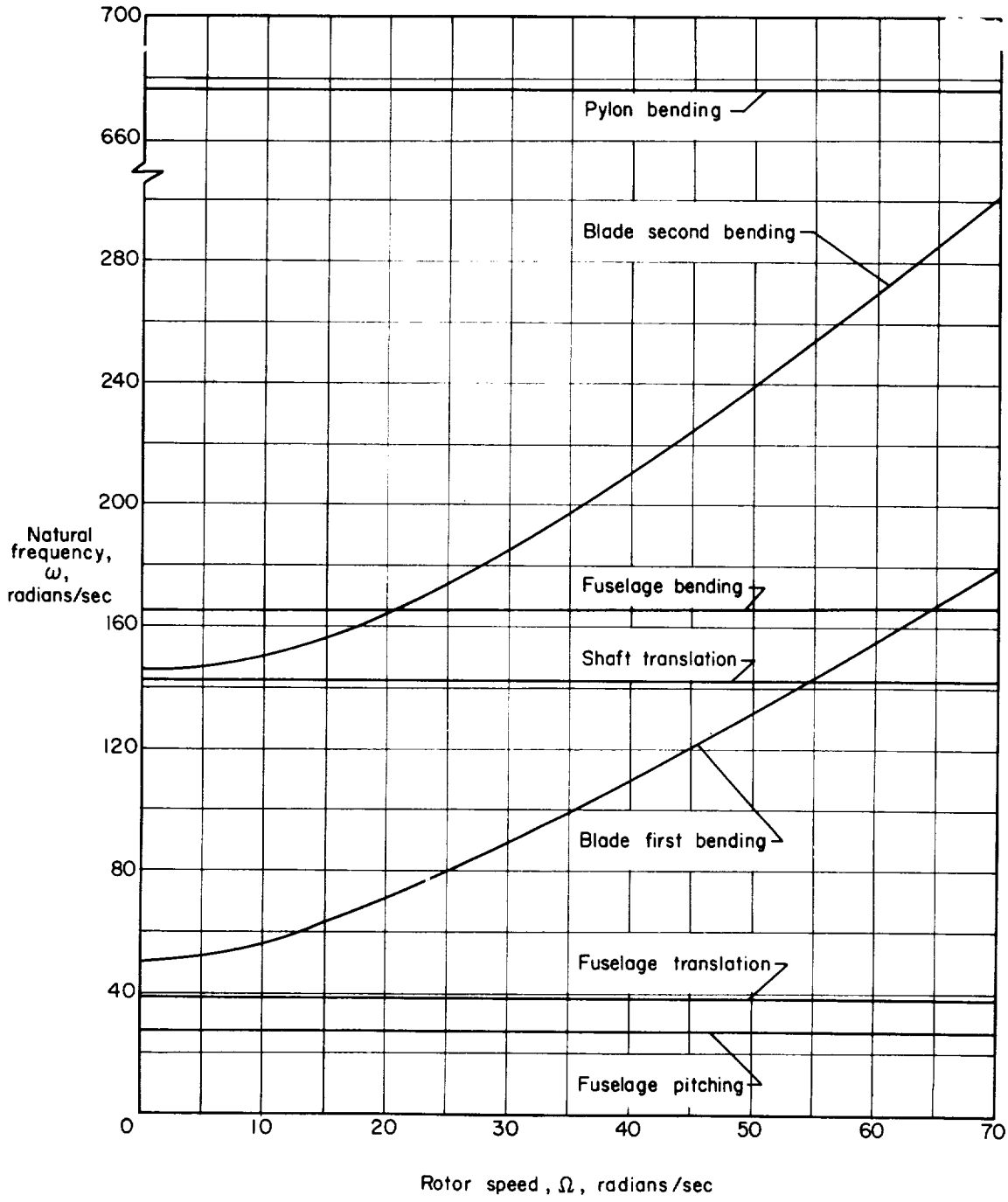

Figure Calculated uncoupled natural frequencies for basic model configuration.

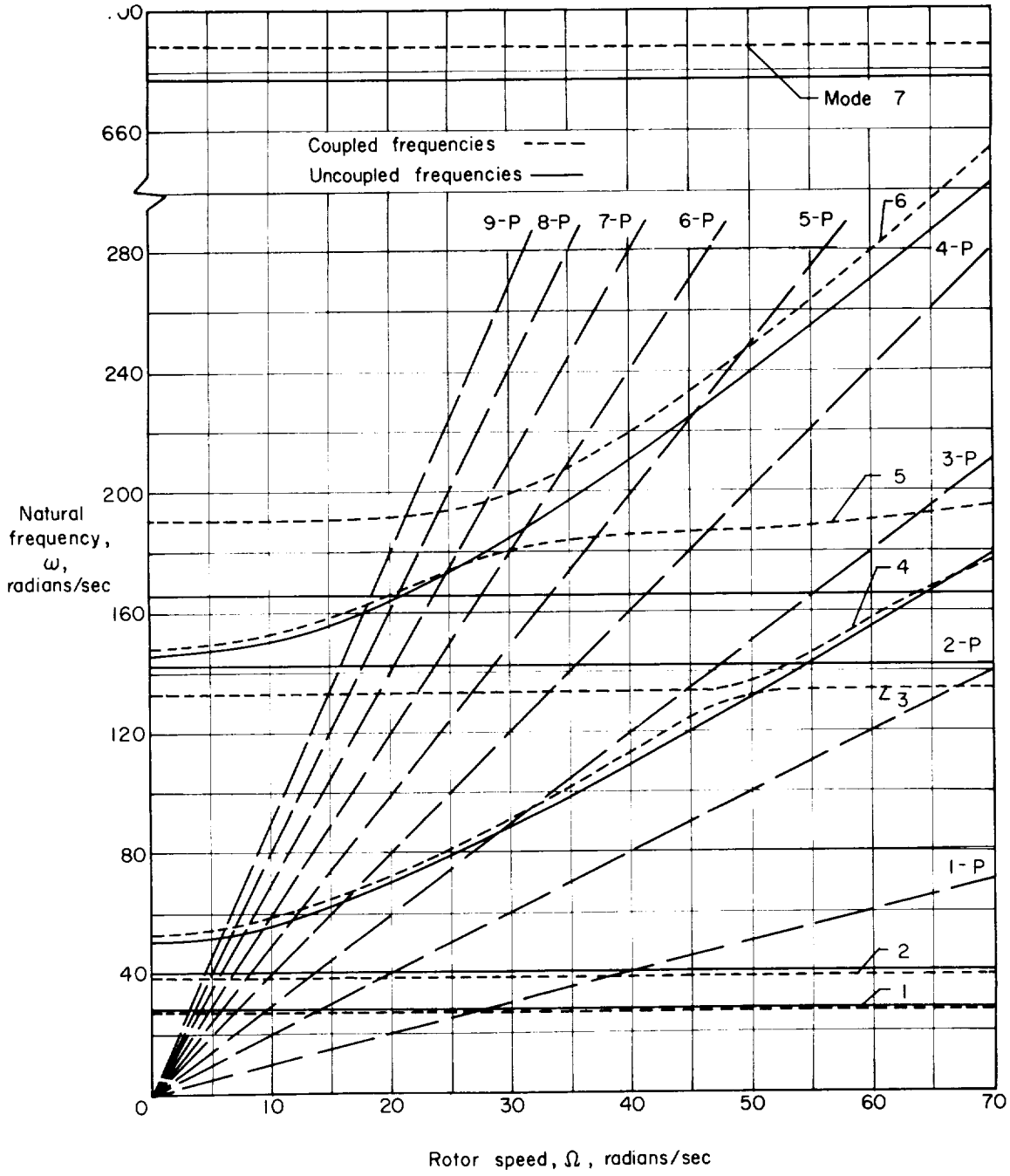

Figure 10.- Comparison of calculated coupled and uncoupled natural f[illegible]ies for the basic model configuration. (1-P, 2-P, etc., represent a 1-per-revolution frequency, a 2-per-revolution fr[illegible]

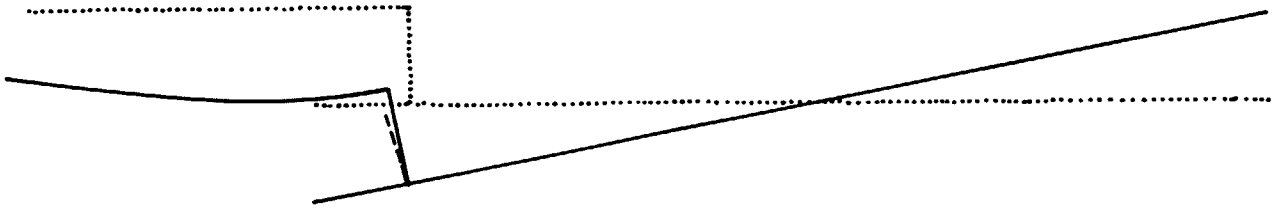

(a) Mode 1. 27.05 radians per second.

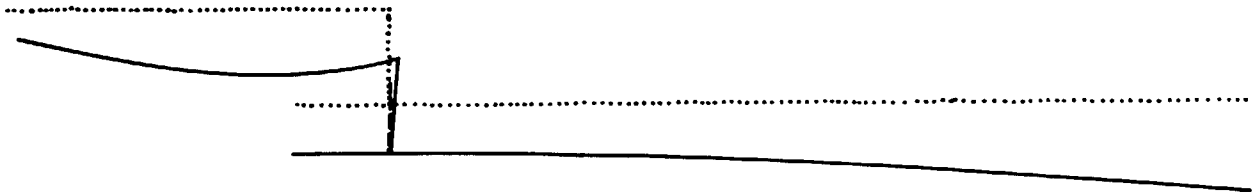

(b) Mode 2. 38.30 radians per second.

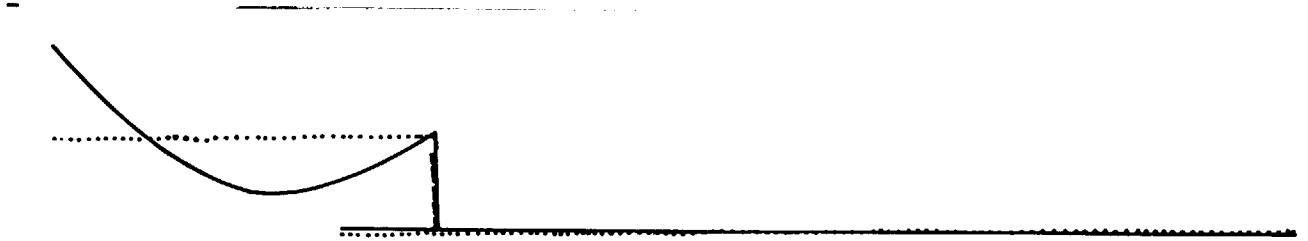

(c) Mode 3. 78.00 radians per second.

Figure 11.- Calculated mode shapes of coupled system. Rotor speed, 23 radians per second; pylon deflections are shown as dashed curves.

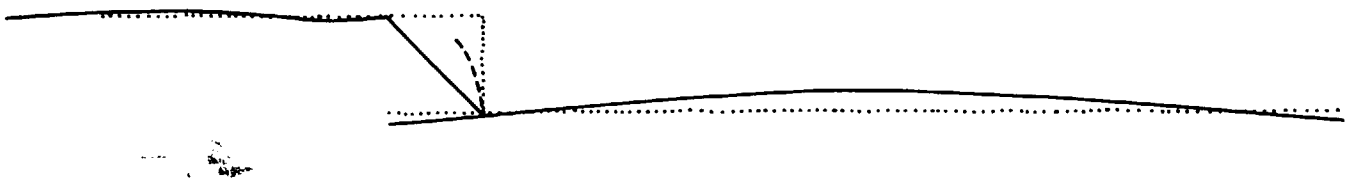

(d) Mode 4. 133.40 radians per second.

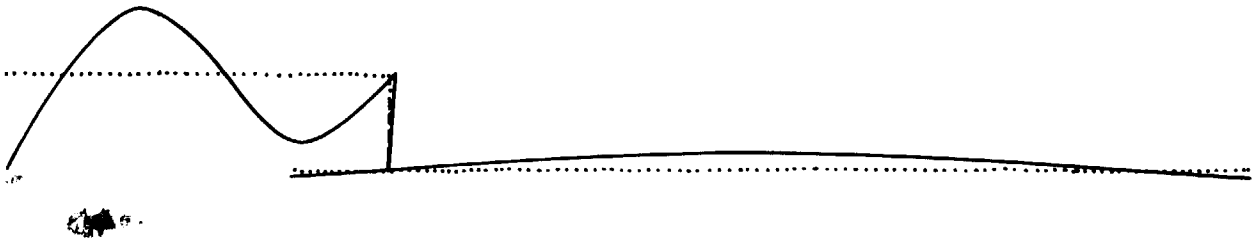

(e) Mode 5. 170.70 radians per second.

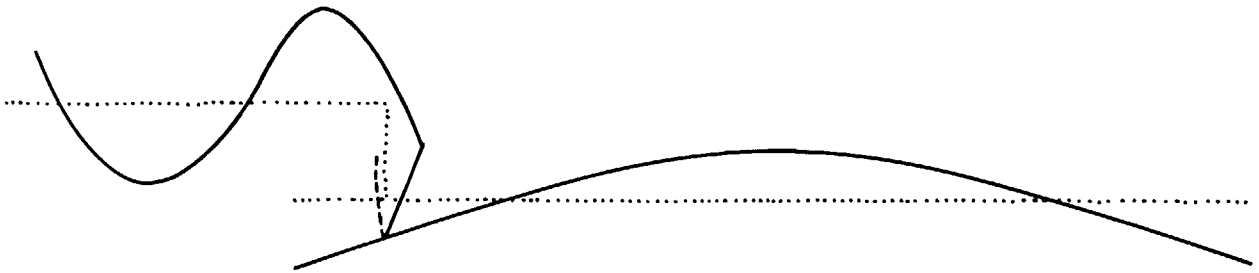

(f) Mode 6. 193.3 radians per second.

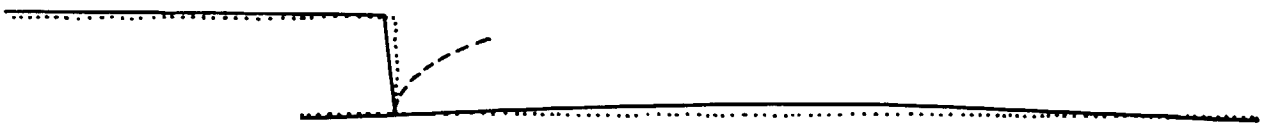

(g) Mode 7. 687.94 radians per second.

Figure 11.- Concluded.

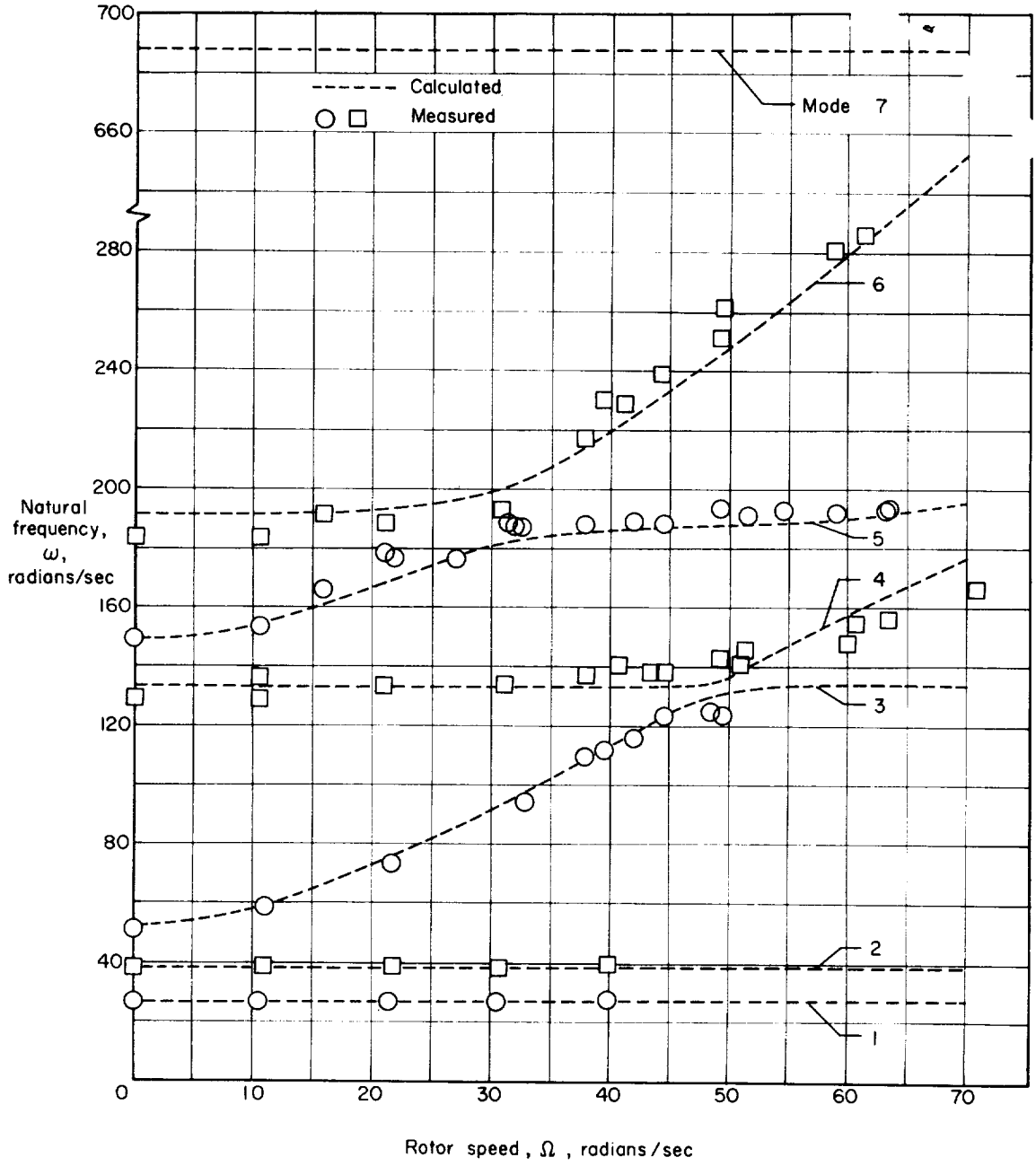

Figure 12.- Comparison of calculated and measured coupled natural frequencies for basic model configuration.

NASA MEMO 11-5-58L
National Aeronautics and Space Administration.
ANALYTICAL AND EXPERIMENTAL DETERMINATION OF THE COUPLED NATURAL FREQUENCIES AND MODE SHAPES OF A DYNAMIC MODEL OF A SINGLE-ROTOR HELICOPTER. Milton A. Silveira and George W. Brooks. December 1958. 42p. diagrs., photos., tabs.
(NASA MEMORANDUM 11-5-58L)

An analytical procedure for the calculation of the coupled natural frequencies and mode shapes in the longitudinal plane of symmetry is presented. The frequencies and mode shapes are then calculated for a dynamic-model helicopter and compared with measured values. The results show good agreement and indicate that the frequencies and mode shapes can be adequately predicted if the structural properties of the helicopter are known.

Copies obtainable from NASA, Washington

1. Wings, Rotating - Experimental Studies (1.6.2)
2. Helicopters (1.7.3.2)
3. Vibration and Flutter - Rotating-Wing Aircraft (4.2.5)
4. Loads and Stresses, Structural - Dynamic (4.3.7.7)

I. Silveira, Milton A.
II. Brooks, George W.
III. NASA MEMO 11-5-58L

NASA

NASA MEMO 11-5-58L
National Aeronautics and Space Administration.
ANALYTICAL AND EXPERIMENTAL DETERMINATION OF THE COUPLED NATURAL FREQUENCIES AND MODE SHAPES OF A DYNAMIC MODEL OF A SINGLE-ROTOR HELICOPTER. Milton A. Silveira and George W. Brooks. December 1958. 42p. diagrs., photos., tabs.
(NASA MEMORANDUM 11-5-58L)

An analytical procedure for the calculation of the coupled natural frequencies and mode shapes in the longitudinal plane of symmetry is presented. The frequencies and mode shapes are then calculated for a dynamic-model helicopter and compared with measured values. The results show good agreement and indicate that the frequencies and mode shapes can be adequately predicted if the structural properties of the helicopter are known.

Copies obtainable from NASA, Washington

1. Wings, Rotating - Experimental Studies (1.6.2)
2. Helicopters (1.7.3.2)
3. Vibration and Flutter - Rotating-Wing Aircraft (4.2.5)
4. Loads and Stresses, Structural - Dynamic (4.3.7.7)

I. Silveira, Milton A.
II. Brooks, George W.
III. NASA MEMO 11-5-58L

NASA

NASA MEMO 11-5-58L
National Aeronautics and Space Administration.
ANALYTICAL AND EXPERIMENTAL DETERMINATION OF THE COUPLED NATURAL FREQUENCIES AND MODE SHAPES OF A DYNAMIC MODEL OF A SINGLE-ROTOR HELICOPTER. Milton A. Silveira and George W. Brooks. December 1958. 42p. diagrs., photos., tabs.
(NASA MEMORANDUM 11-5-58L)

An analytical procedure for the calculation of the coupled natural frequencies and mode shapes in the longitudinal plane of symmetry is presented. The frequencies and mode shapes are then calculated for a dynamic-model helicopter and compared with measured values. The results show good agreement and indicate that the frequencies and mode shapes can be adequately predicted if the structural properties of the helicopter are known.

Copies obtainable from NASA, Washington

1. Wings, Rotating - Experimental Studies (1.6.2)
2. Helicopters (1.7.3.2)
3. Vibration and Flutter - Rotating-Wing Aircraft (4.2.5)
4. Loads and Stresses, Structural - Dynamic (4.3.7.7)

I. Silveira, Milton A.
II. Brooks, George W.
III. NASA MEMO 11-5-58L

NASA

NASA MEMO 11-5-58L
National Aeronautics and Space Administration.
ANALYTICAL AND EXPERIMENTAL DETERMINATION OF THE COUPLED NATURAL FREQUENCIES AND MODE SHAPES OF A DYNAMIC MODEL OF A SINGLE-ROTOR HELICOPTER. Milton A. Silveira and George W. Brooks. December 1958. 42p. diagrs., photos., tabs.
(NASA MEMORANDUM 11-5-58L)

An analytical procedure for the calculation of the coupled natural frequencies and mode shapes in the longitudinal plane of symmetry is presented. The frequencies and mode shapes are then calculated for a dynamic-model helicopter and compared with measured values. The results show good agreement and indicate that the frequencies and mode shapes can be adequately predicted if the structural properties of the helicopter are known.

Copies obtainable from NASA, Washington

1. Wings, Rotating - Experimental Studies (1.6.2)
2. Helicopters (1.7.3.2)
3. Vibration and Flutter - Rotating-Wing Aircraft (4.2.5)
4. Loads and Stresses, Structural - Dynamic (4.3.7.7)

I. Silveira, Milton A.
II. Brooks, George W.
III. NASA MEMO 11-5-58L

NASA